

Probing few-excitation eigenstates of interacting atoms on a lattice by observing their collective light emission in the far field

Paolo Longo* and Jörg Evers

Max Planck Institute for Nuclear Physics, Saupfercheckweg 1, 69117 Heidelberg, Germany

(Dated: February 29, 2024)

The collective emission from a one-dimensional chain of interacting two-level atoms coupled to a common electromagnetic reservoir is investigated. We derive the system's dissipative few-excitation eigenstates, and analyze its static properties, including the collective dipole moments and branching ratios between different eigenstates. Next, we study the dynamics, and characterize the light emitted or scattered by such a system via different far-field observables. Throughout the analysis, we consider spontaneous emission from an excited state as well as two different pump field setups, and contrast the two extreme cases of non-interacting and strongly interacting atoms. For the latter case, the two-excitation submanifold contains a two-body bound state, and we find that the two cases lead to different far-field signatures. Finally we exploit these signatures to characterize the wavefunctions of the collective eigenstates. For this, we identify a direct relation between the collective branching ratio and the momentum distribution of the collective eigenstates' wavefunction. This provides a method to proof the existence of certain collective eigenstates and to access their wave function without the need to individually address and/or manipulate single atoms.

PACS numbers: 42.50.Nn, 42.50.Ct

I. INTRODUCTION

In recent years, tailored lattice systems of (artificial) atoms have turned into a thriving field of experimental and theoretical research across many different subdisciplines of quantum optics. Still, the typical questions and problems addressed in the context of atomic lattice systems interacting with light often relate to basic and generic properties. Physical realizations of artificial atomic lattice systems cover a wide range of technologies with which light-matter interactions can be studied. To name just a few, these include cold atoms in optical lattices [1–3], fiber-based settings [4], atom-cavity networks and on-chip photonics [5–8], or cold polar molecules [9].

One particular line of research involves static and dynamic properties of the system in the few-excitation subspace [10, 11, 15, 16]. In particular few-excitation eigenstates in one dimension are also connected to the topic of more “exotic” eigenstates such as two-body bound states on a lattice [1, 2, 10, 11, 16, 17]. These represent a nice example for how a “historical” prediction originally put forward by Bethe [18] is investigated today by means of cutting-edge experimental techniques [1, 2].

However, oftentimes, related experiments are very demanding in that they require *in situ* tuning of parameters and/or rely on single-site manipulation. This motivates alternative approaches such as the coupling to a probing light field [17, 19–23]. Essentially, the key question here is about how much information on the eigenstates of an atomic lattice system can be inferred from the scattered light in the far field when the system is probed optically.

A recent addition to the zoo of lattice systems arises from the emerging field of x-ray quantum optics [24]. Nu-

clear transitions driven, e.g., by synchrotron light [25], are a particularly promising implementation, fueled by a number of recent theoretical [26–32] and experimental [33–42] works. Typically, the nuclei are embedded in a solid state target, which may exhibit a crystalline structure. Facilitated by the Mößbauer effect [43, 44], suitable nuclei such as ^{57}Fe have the additional benefit of offering recoil-less absorption or emission of light. Nanostructuring of the target, e.g., into thin-film waveguide structures [32, 36, 38, 39] or nano-wires [41], allows one to explore lower-dimensional geometries. Furthermore, in state-of-the-art experiments, source limitations naturally restrict the nuclei to the low-excitation subspace. Finally, since the nuclei are probed via scattered light observed in the far field, again the question arises, how much this light reveals about the system.

Motivated by this question, here, we study the far-field signatures that emerge in the collective emission from dipole-dipole coupled two-level atoms on a one-dimensional lattice (see Fig. 1). To this end, we develop an analytical framework reminiscent of spin physics, which allows us to discuss the relevant physical mechanisms in a broader context. We start by deriving the dissipative few-excitation eigenstates of the coupled atoms subject to a common reservoir. Next, we determine the collective dipole moments and related branching ratios for transitions between the eigenstates of the atomic chain. As a key result of this analysis, we identify a connection between the momentum distribution of the collective atomic states' wavefunctions and these branching ratios. This analysis further enables us to determine the relevant level space for the spontaneous emission from an excited eigenstate, as well as under the influence of weak incoherent driving fields. We then study the dynamics within this relevant level space by means of a master equation. Relating the electric far field operator to

* paolo.longo@mpi-hd.mpg.de

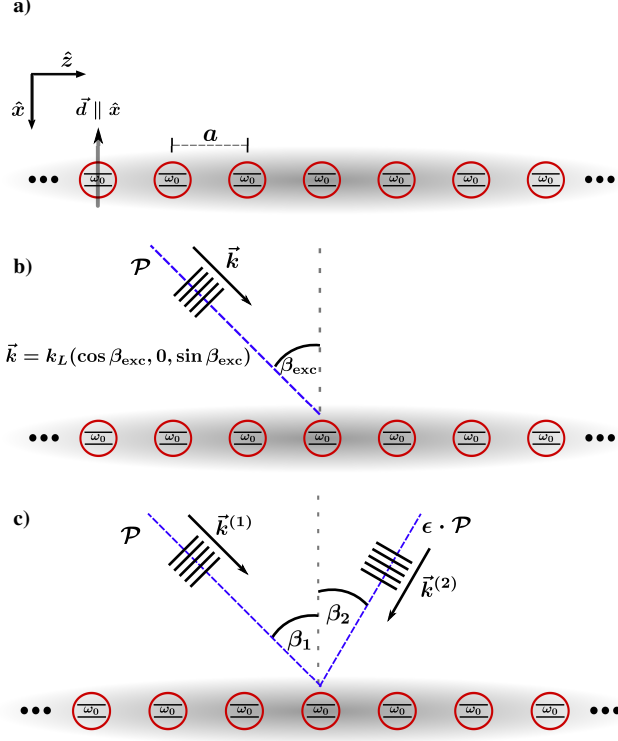


FIG. 1. (color online) General structure of the analysis. (a) shows the basic setup. The two-level atoms (bare transition energy ω_0) are arranged on a one-dimensional lattice (lattice constant a) along the z direction. The atoms' dipole moments are uniformly aligned and lie in the x - z plane (in this sketch, we have exemplarily chosen an angle between the dipole moments and the atomic chain of $\theta = \pi/2$). The whole chain is coupled to a common reservoir indicated by the shading. In (b), the first considered pump-field configuration is shown, with an incoherent pump rate $|\mathcal{P}|^2$ applied at an excitation angle β_{exc} . The pump's electric field polarization vector lies in the x - z plane and is perpendicular to the driving field's wave vector \mathbf{k} . To separate the scattered field from the driving field, a detection out-of-plane (i. e., in the y - z plane) could be performed. (c) Two-pump setup with excitation angles β_1 and β_2 . The ratio of the driving fields' pump rates is ϵ^2 .

the collective atomic eigenbasis, we can evaluate far-field observables such as the emitted intensity, the emission spectrum, and an intensity correlation function. This approach is of interest since it does not require single-atom addressability or manipulation techniques, and it is compatible with recent experiments in nuclear quantum optics.

In our analysis, we particularly contrast the two extreme cases of non-interacting and strongly interacting atoms. For the latter case, the two-excitation submanifold comprises not only scattering states but also two-body bound states of atomic excitation. We further find that the two cases lead to different dynamics, involving characteristic branching ratios between the eigenstates. These differences also manifest themselves in all optical

far-field observables. As an application, we discuss different driving field setups to characterize the collective eigenstates' wavefunctions via the scattered light. Finally, as an outlook, we calculate second-order correlation functions of the light in the far field.

This paper is organized as follows. In Sec. II, we introduce our model and discuss its static properties. Furthermore, we determine the electric far-field operator in the collective atomic eigenbasis and define our observables. Based on a Lindblad master equation, we analyze in Sec. III the angle-dependent far-field pattern emerging from the spontaneous emission of the system's eigenstates. In Sec. IV, we discuss the far-field properties in the presence of external driving fields. We conclude the paper in Sec. V. Appendices A–G provide technical details on the calculations performed.

II. FUNDAMENTALS

A. The Model

We start with the Hamiltonian ($\hbar \equiv 1$) of $M \equiv N + 1 \gg 1$ (N is even) two-level atoms that are periodically arranged on a one-dimensional lattice (lattice constant a), are linearly coupled to a photon bath, and are subject to a pair interaction $V_{nm} = V_{|n-m|}$ (where $V_0 = 0$):

$$\begin{aligned}
 H = & \sum_{n=-\frac{N}{2}}^{\frac{N}{2}} \omega_n \sigma_n^+ \sigma_n^- + \sum_k \epsilon_k a_k^\dagger a_k \\
 & + \sum_{n=-\frac{N}{2}}^{\frac{N}{2}} \sum_k \left(g_{nk} \sigma_n^+ a_k + g_{nk}^* \sigma_n^- a_k^\dagger \right) \\
 & + \frac{1}{2} \sum_{n=-\frac{N}{2}}^{\frac{N}{2}} \sum_{m=-\frac{N}{2}}^{\frac{N}{2}} V_{|n-m|} \sigma_n^+ \sigma_n^- \sigma_m^+ \sigma_m^-.
 \end{aligned} \tag{1}$$

The atomic indices refer to lattice sites, $\omega_n = \omega_0 \forall n$ denotes the atomic transition energies, and g_{nk} signifies the coupling of atom n to mode k of a photon bath (whose dispersion relation is ϵ_k). The photonic creation and annihilation operators a_k^\dagger and a_k are bosonic operators and the index k runs over all modes of the photon reservoir. The atomic raising (lowering) operator of atom n is denoted by σ_n^+ (σ_n^-), satisfying the commutation relation $[\sigma_n^+, \sigma_m^-] = \delta_{nm} \sigma_n^z$, where $\sigma_n^+ = |\uparrow\rangle_n \langle \downarrow|_n$, $\sigma_n^- = (\sigma_n^+)^\dagger$, and $\sigma_n^z = |\uparrow\rangle_n \langle \uparrow|_n - |\downarrow\rangle_n \langle \downarrow|_n$. Here, $|\uparrow\rangle_n$ ($|\downarrow\rangle_n$) denotes the excited (ground) state of atom n .

Upon eliminating the photonic degrees of freedom similarly to the formalism presented in Ref. [45] (see App. A for details), we arrive at the effective, non-Hermitian

Hamiltonian

$$H_{\text{eff}} = \sum_{n=-\frac{N}{2}}^{\frac{N}{2}} \omega_0 \sigma_n^+ \sigma_n^- - \frac{i}{2} \sum_{n=-\frac{N}{2}}^{\frac{N}{2}} \sum_{m=-\frac{N}{2}}^{\frac{N}{2}} \Gamma_{|n-m|} \sigma_n^+ \sigma_m^- + \frac{1}{2} \sum_{n=-\frac{N}{2}}^{\frac{N}{2}} \sum_{m=-\frac{N}{2}}^{\frac{N}{2}} V_{|n-m|} \sigma_n^+ \sigma_n^- \sigma_m^+ \sigma_m^-. \quad (2)$$

The individual terms in this Hamiltonian can be understood as follows. Being coupled to an electromagnetic reservoir, an individual atom experiences an energy shift (Lamb shift) of $\text{Im}(\Gamma_0)/2$ and it is subject to spontaneous decay at a rate of $\text{Re}(\Gamma_0) \equiv \gamma_0$. Photons can be exchanged between nearby atoms via the common electromagnetic reservoir by virtue of dipole-dipole coupling. These processes are incorporated into the terms with $\text{Im}(\Gamma_{|n-m| \geq 1})$, while the dissipative part (i.e., $\text{Re}(\Gamma_{|n-m| \geq 1})$) leads to a modification of the spontaneous emission rate. Furthermore, two atoms at a relative distance of $|n-m|a$ experience an interaction-induced energy shift $V_{|n-m|}$ if they are both in the excited state. Hamiltonian (2) can also be seen as describing interacting and dissipative spin-1/2 excitations on a one-dimensional lattice.

In this paper, we aim at investigating the regime of an extended sample, where the bare atomic emission wavelength $\lambda_{\text{at}} = 2\pi/k_{\text{at}} = 2\pi c/\omega_0$ (c is the speed of light) is smaller than the lattice constant, i.e., $\lambda_{\text{at}}/a < 1$, contrasting the established “small-volume limit” originally investigated by Dicke [46, 47]. In the following, we restrict the dipole-dipole coupling and the atom-atom interactions to nearest neighbors. The only parameters left in this regime are Γ_0 , Γ_1 , and $U \equiv V_1$, resulting in the tight-binding formulation

$$H_{\text{eff}}^{\text{tb}} = \sum_{n=-\frac{N}{2}}^{\frac{N}{2}} \left(\omega_0 - \frac{i\Gamma_0}{2} \right) \sigma_n^+ \sigma_n^- - \frac{i\Gamma_1}{2} \sum_{n=-\frac{N}{2}}^{\frac{N}{2}-1} (\sigma_{n+1}^+ \sigma_n^- + \text{h.c.}) + U \sum_{n=-\frac{N}{2}}^{\frac{N}{2}-1} \sigma_{n+1}^+ \sigma_{n+1}^- \sigma_n^+ \sigma_n^-. \quad (3)$$

For atoms coupled to free space, the complex rates that enter Hamiltonians (2) and (3) are given by [45]

$$\frac{\Gamma_0}{\gamma_0} = 1 - \frac{2i}{\pi}, \quad (4)$$

$$\frac{\Gamma_{x \neq 0}}{\gamma_0} = A_x \sin^2 \theta + B_x \cdot \frac{3 \cos^2 \theta - 1}{2}, \quad (5)$$

$$A_x = -\frac{3ie^{i\xi_x}}{2\xi_x}, \quad (6)$$

$$B_x = \frac{3}{\xi_x^3} \cdot [\sin \xi_x - \xi_x \cos \xi_x]$$

$$- i(\cos \xi_x + \xi_x \sin \xi_x)], \quad (7)$$

$$\xi_x = k_{\text{at}} a |x| = \omega_0 a |x| / c, \quad (8)$$

where $x \equiv n - m$ and θ denotes the angle between the atomic chain (z axis) and the atomic dipole moment \mathbf{d} (see also Fig. 1a)).

Exemplarily, orders of magnitudes in the field of Rydberg atoms trapped in an optical lattice are [48] $\lambda_{\text{at}} \sim 500$ nm, $(\omega_0/2\pi \sim 500$ THz), $\gamma_0 \sim$ MHz, and $U \sim 50$ GHz (for $a \sim 1$ μm), representing separated scales $\omega_0 \gg U \gg \gamma_0$. Alternatively, in the realm of x-ray quantum optics [33–41], for instance the ^{57}Fe Mössbauer transition is characterized by $\omega_0/2\pi \sim 10^{18}$ Hz, $\gamma_0 \sim$ MHz, $a \sim$ pm, and $U = 0$. For these systems, crystalline solid state targets naturally provide ordered arrays of x-ray emitters.

B. Eigenstates and Eigenvalues

In this Section, we investigate the non-Hermitian eigenvalue problem

$$(H_{\text{eff}} - E) |\Psi\rangle = 0. \quad (9)$$

The resulting eigenvalues E are complex and the real part plays the role of the eigenstate’s excitation energy, whereas $-2\text{Im}(E)$ can be interpreted as the decay rate of the eigenstate’s occupation number [45]. Also note that for a non-Hermitian Hamiltonian, the left eigenstates are in general not just the Hermitian conjugate of the right eigenstates (as it would be for a Hermitian Hamiltonian). Generally, the notion of biorthogonality needs to be taken into account (for instance, see Ref. [49]). However, these details will not be important in the course of this paper since we are led by the following train of thought.

First, we use an effective non-Hermitian Hamiltonian to obtain the energies and decay rates in the system’s eigenbasis. Later on, when switching to a Lindblad formulation (Sec. III A), the coherent time evolution is given with respect to the “closed” system described by the Hermitian part of the Hamiltonian which is realized formally by setting the real parts of the complex rates to zero, i.e., $\text{Re}(\Gamma_x) = 0$. Note that setting the real part of the complex decay rates to zero results in a Hermitian Hamiltonian, yielding real energy eigenvalues (which are the system’s transition energies). Expressed differently, the coherent part of the Lindblad equation is diagonal with respect to the “non-dissipative” basis (which we also utilize for the calculation of matrix elements). Likewise, the dissipators in the incoherent part of the Lindblad equation contain the eigenstates’ total decay rates as obtained from the imaginary part of the complex eigenenergies of the original non-Hermitian Hamiltonian [50].

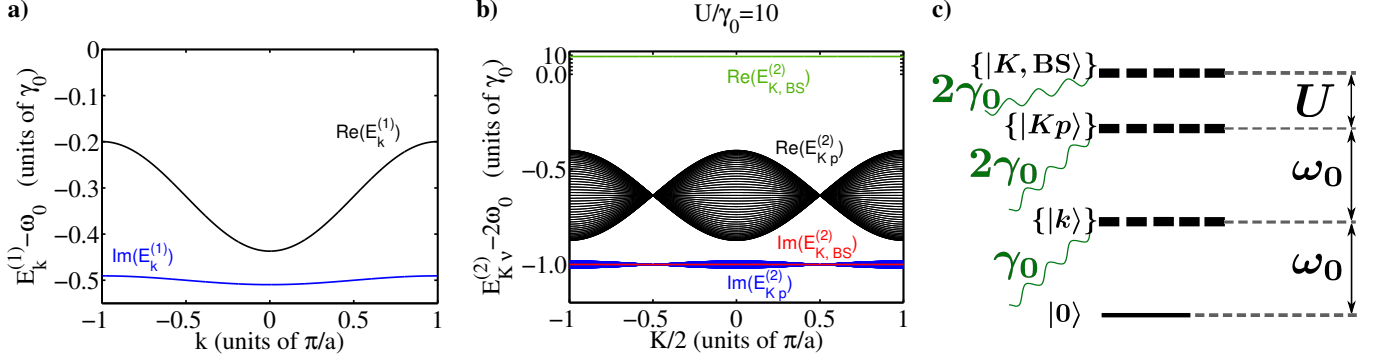


FIG. 2. (color online). Complex dispersion relations for single-excitation states $|k\rangle$ (a)) and two-excitation states $|K\nu\rangle$ (b)). Note that the energies of the bound states are detached from the quasicontinuum of scattering states. The parameters chosen here are $\lambda_{\text{at}}/a = 0.5$ and $\theta = \pi/2$, resulting in $\Gamma_0/\gamma_0 = 1 - 0.637i$ and $\Gamma_1/\gamma_0 = 0.009 - 0.119i$. For $\omega_0 \gg U \gg \gamma_0$, we can resort to a simplified level scheme of quasidegenerate bands (c)).

1. Single-Excitation Eigenstates and Eigenvalues

A solution to the single-excitation eigenproblem (see App. B 1 for details) can be formulated in terms of a Bloch wave

$$|k\rangle = \sum_n \frac{e^{ikan}}{\sqrt{M}} \sigma_n^+ |0\rangle, \quad (10)$$

where $ka = -\pi + 2\pi\ell/M$ ($\ell = 0, 1, \dots, M-1$) is a wavenumber from the first Brillouin zone and $|0\rangle$ signifies the vacuum state. The complex eigenvalues for the general Hamiltonian (2) are essentially given as the Fourier lattice transform of the complex rates, i.e.,

$$\begin{aligned} E_k^{(1)} &= \omega_0 - \frac{i}{2} \sum_{x=-\frac{N}{2}}^{\frac{N}{2}} \Gamma_x e^{-ikax} \\ &= \omega_0 - \frac{i}{2} \Gamma_0 - i \sum_{x=1}^{\frac{N}{2}} \Gamma_x \cos(kax). \end{aligned} \quad (11)$$

Rewritten in terms of the collective Lamb shift and decay rate we have

$$\begin{aligned} \text{Re}(E_k^{(1)}) &= \omega_0 + \frac{1}{2} \text{Im}(\Gamma_0) + \sum_{x=1}^{\frac{N}{2}} \text{Im}(\Gamma_x) \cos(kax), \quad (12) \\ \Gamma_k &\equiv -2\text{Im}(E_k^{(1)}) = \gamma_0 + 2 \sum_{x=1}^{\frac{N}{2}} \text{Re}(\Gamma_x) \cos(kax) \end{aligned}$$

As a side note we would like to point out that the superradiant Dicke state [46, 47] in the small-volume limit $a \rightarrow 0$ is also accounted for in the above expressions. For $a \rightarrow 0$, we have $\Gamma_x \rightarrow \Gamma_0$ (see Eqs. (4)–(8)) so that the state with $k = 0$ (symmetric Dicke state) exhibits a decay rate as well as a Lamb shift proportional to the number of emitters M in the volume. Hence, $\Gamma_{k=0} \xrightarrow{a \rightarrow 0} M\gamma_0$ and $\text{Re}(E_k^{(1)} = 0) \xrightarrow{a \rightarrow 0} \omega_0 - M\gamma_0/\pi$.

However, for the remainder of this paper, we focus on the regime of an extended sample and utilize the tight binding Hamiltonian (3). In that case, the above formulae reduce to

$$\text{Re}(E_k^{(1)}) = \omega_0 + \frac{1}{2} \text{Im}(\Gamma_0) + \text{Im}(\Gamma_1) \cos(ka) \simeq \omega_0 \quad (14)$$

$$\Gamma_k = \gamma_0 + 2\text{Re}(\Gamma_1) \cos(ka) \simeq \gamma_0, \quad (15)$$

where the approximated expressions are valid for $\gamma_0/\omega_0 \ll 1$, describing sharp optical resonances. The single-excitation dispersion relation for the tight-binding case is depicted in Fig. 2a).

2. Two-Excitation Eigenstates and Eigenvalues

The solution to the two-excitation problem (see App. B 2 for details) can be written in terms of a product of the center-of-mass motion (described by a plane wave with a center-of-mass wavenumber K) and a relative wavefunction $\Psi_{|n_1-n_2|}^{(K\nu)}$, i.e.,

$$|K\nu\rangle = \frac{1}{2\sqrt{M}} \sum_{n_1 n_2} e^{i\frac{K a}{2}(n_1+n_2)} \cdot \Psi_{|n_1-n_2|}^{(K\nu)} \sigma_{n_1}^+ \sigma_{n_2}^+ |0\rangle. \quad (16)$$

Here, $K/2$ is from the first Brillouin zone and ν is a quantum number still to be determined. For $n_1 = n_2$, the wavefunction needs to vanish ($\Psi_0^{(K\nu)} = 0$) since a single atom cannot be doubly excited, expressing the fact that the excitations of a 1D spin-1/2 chain are hard-core bosons.

Note that this eigenproblem is similar to the problem of two excitations in the extended Bose-Hubbard model [10, 11] and also occurs in the study of biexcitons in arrays of coupled chromophores [12–14]. Originally put forward by Bethe [18] (and, for instance, also addressed in Refs. [1, 2, 10, 11, 16, 18]), is the remarkable fact that a complete basis of the two-excitation submanifold com-

prises scattering states *and* bound states. We will now discuss these two classes of solutions.

Scattering States.— For each center-of-mass wavenumber K , we have scattering states characterized by their relative wavenumber p (from the first Brillouin zone). The relative wave function is of the form ($x \neq 0$)

$$\Psi_x^{(Kp)} = \frac{1}{\sqrt{M}} \left(e^{ipa|x|} + e^{i\delta_{Kp}} e^{-ipa|x|} \right), \quad (17)$$

where δ_{Kp} is the scattering phase shift due to the atom-atom interaction. The corresponding complex energy eigenvalues can be written as

$$\begin{aligned} \text{Re}(E_{Kp}^{(2)}) &= 2\omega_0 + \text{Im}(\Gamma_0) + 2\text{Im}(\Gamma_1) \cos\left(\frac{Ka}{2}\right) \cos(pa) \\ &\simeq 2\omega_0, \end{aligned} \quad (18)$$

$$\begin{aligned} \Gamma_{\text{tot}}^{Kp} &\equiv -2\text{Im}(E_{Kp}^{(2)}) \\ &= 2\gamma_0 + 4\text{Re}(\Gamma_1) \cos\left(\frac{Ka}{2}\right) \cos(pa) \\ &\simeq 2\gamma_0. \end{aligned} \quad (19)$$

This two-excitation dispersion relation is depicted in Fig. 2b). As in Eqs. (14) and (15), the approximated expressions are valid for $\gamma_0/\omega_0 \ll 1$. Note that the eigenvalues (18) and (19) do not depend on the scattering potential U . In fact, the (complex) eigenenergy is just the energy of the “free” particles as it is always the case in scattering theory. This becomes most apparent when expressing the center-of-mass and the relative wavenumbers in terms of single-particle wavenumbers k_1 and k_2 , i. e., $E_{Kp}^{(2)} = E_{k_1+k_2, (k_1-k_2)/2}^{(2)} = E_{k_1}^{(1)} + E_{k_2}^{(1)}$. In particular, when there is no interaction ($U = 0$) the full many-body solution can be written as a direct product of single-excitation states and the many-body eigenenergy is the sum of the single-excitation energies.

In the introduction of Sec. II B, we mentioned that the eigenstate’s wavefunction coefficients belonging to the non-dissipative, Hermitian system (realized by setting $\text{Re}(\Gamma_0) = \text{Re}(\Gamma_1) = 0$) are important for a later calculation of matrix elements. The corresponding scattering phase shift for the non-dissipative system is [51]

$$e^{i\delta_{Kp}} = -\frac{\text{Im}(\Gamma_1) \cos\left(\frac{Ka}{2}\right) - Ue^{ipa}}{\text{Im}(\Gamma_1) \cos\left(\frac{Ka}{2}\right) - Ue^{-ipa}}. \quad (20)$$

For the remainder of this paper, we will concentrate on the two cases of non-interacting atoms ($U = 0$) and strong atom-atom interactions (“large U limit”). For $U = 0$ the phase shift is

$$e^{i\delta_{Kp}} = -1 \quad (U = 0). \quad (21)$$

This is a result of the hard-core constraint $\Psi_0^{(K\nu)} = 0$ and can be understood as an infinite repulsion at zero relative coordinate. Conversely, in the limit of strong atom-atom interactions, where $U \gg \gamma_0 > \text{Im}(\Gamma_1)$, the phase shift is

$$e^{i\delta_{Kp}} = -e^{2ipa} \quad (U \gg \gamma_0). \quad (22)$$

Further note that, for both $U = 0$ and large U , the $p = 0$ -wavefunction vanishes. This also includes the so-called symmetric Dicke state with $K = p = 0$ for which the relative phases between the different wavefunction coefficients is constant. Unlike for the original Dicke model, two excitations in our tight-binding model interfere destructively for $p = 0$ due to the mentioned hard-core constraint (see $e^{i\delta_{Kp}} = -1$ in Eqs. (21), (22), and (17)).

Bound States.— Additionally, the system may also feature bound states [10, 11, 16], whose relative wavefunction is of the form ($x \neq 0$)

$$\Psi_x^{(K, \text{BS})} = \alpha_K^{|x|-1}, \quad (23)$$

where $\alpha_K = -i\Gamma_1 \cos\left(\frac{Ka}{2}\right)/U$ and the complex energy eigenvalues are

$$\text{Re}(E_{K, \text{BS}}^{(2)}) = 2\omega_0 + \text{Im}(\Gamma_0) + U \quad (24)$$

$$\begin{aligned} & - \cos^2\left(\frac{Ka}{2}\right) \cdot \frac{[(\text{Re}(\Gamma_1))^2 - (\text{Im}(\Gamma_1))^2]}{U} \\ & \simeq 2\omega_0 + U, \\ \Gamma_{\text{tot}}^{K, \text{BS}} & \equiv -2\text{Im}(E_{K, \text{BS}}^{(2)}) \\ & = 2\gamma_0 + 4 \cos^2\left(\frac{Ka}{2}\right) \cdot \frac{\text{Re}(\Gamma_1)\text{Im}(\Gamma_1)}{U} \\ & \simeq 2\gamma_0. \end{aligned} \quad (25)$$

Again, the approximated expressions are valid for $\omega_0 \gg U \gg \gamma_0$, i. e., for sharp optical resonances and strong atom-atom interactions. The dispersion relation for the two-body bound states is compared with the scattering states’ properties in Fig. 2b). Figure 2c) summarizes the few-excitation Hilbert space in terms of a simplified level scheme consisting of quasi-degenerate bands (which is valid for $\omega_0 \gg \gamma_0$).

Note that—in contrast to the scattering states—the energy of the bound states also depends on the dissipative property $\text{Re}(\Gamma_1)$. This can be understood as a dissipation-induced energy shift due to the dressing of the bound state through the reservoir. However, this effect is negligible for strong atom-atom interactions $U \gg \gamma_0$.

If we, as before, imagine the non-dissipative system (where $\text{Re}(\Gamma_0) = \text{Re}(\Gamma_1) = 0$) and require the relative wavefunction to be spatially confined, the condition $|\alpha_K| < 1$ translates into

$$\left| \text{Im}(\Gamma_1) \cos\left(\frac{Ka}{2}\right) \right| < |U|. \quad (26)$$

This criterion for the existence of a two-body bound state with a center-of-mass wavenumber K is always fulfilled for $U \gg \gamma_0$. In this regime of strong atom-atom interactions, the two-body bound state is tightly confined with respect to the relative coordinate, i. e.,

$$\Psi_x^{(K, \text{BS})} = \delta_{|x|,1} \quad (U \gg \gamma_0), \quad (27)$$

describing a composite two-excitation object moving along the lattice. Because only neighboring sites are occupied here, the minimal spatial separation between two excitations is given by the lattice constant a .

The nearest neighbor interaction U can be understood as the discrete variant of a δ -like potential. Therefore, for each center-of-mass wavenumber K , there is at most one bound state in the spectrum. There are no bound states in the case of non-interacting atoms ($U = 0$).

When comparing the complex eigenenergies of scattering states and bound states, we find that two excitations approximately all decay at a rate of $\Gamma_{\text{tot}}^{K\nu} \simeq 2\gamma_0$ (for both $\nu = p$ and $\nu = \text{BS}$). However, the bound states' energies are detached from the quasicontinuum of scattering states due to an interaction induced shift which is on the order of U (see also Fig. 2).

C. Collective Dipole Moments and Momentum Distribution

We now turn to the problem of how in detail a two-excitation eigenstate decays (cf. Fig. 3a)) and show that the relevant key quantity here is intimately linked to the state's momentum distribution.

1. Dipole Moments and Branching Ratio

As the effective Hamiltonian (2) lacks the detailed information of the various possible decay paths (degrees of freedom have been integrated out), we need to consider the collective operator

$$\begin{aligned} D^- &= \sum_{\mu} \sum_{y=-\frac{N}{2}}^{\frac{N}{2}} D_{y\mu}^-, \\ D_{y\mu}^- &= g_{y\mu}^* \sigma_y^- a_{\mu}^{\dagger} \\ &= g_{\mu}^* \frac{e^{-i\mu ay}}{\sqrt{M}} \sigma_y^- a_{\mu}^{\dagger}, \end{aligned} \quad (28)$$

which induces one-photon transitions. Here, g_{μ} signifies the atom-photon coupling strength (which can be considered being wave number independent across the spectral window that is relevant here), and μ denotes the wavenumber that is transferred to the photon field. This collective operator transfers a collective n -excitation atomic state to the sub-manifold of $n - 1$ excitations, which is accompanied by the emission of a photon.

To identify the possible decay paths, we calculate the transition matrix elements $\sum_f \langle f | D^- | i \rangle$ with respect to the non-dissipative eigenstates (as explained in the introduction of Sec. II B). As an initial state, we take the direct product of the photon reservoir being in the vacuum state and the atomic system being in a two-excitation eigenstate, i.e., $|i\rangle = |K\nu\rangle \otimes |\{0\}\rangle$. Consequently, the target states $|f\rangle = |k\rangle \otimes |1_{\mu}\rangle$ consist of an atomic single-excitation state and a single photon (in mode μ). Explicit

calculation reveals that

$$\begin{aligned} \sum_f \langle f | D^- | i \rangle &= \sum_{\mu} \sum_y g_{\mu}^* \frac{e^{-i\mu ay}}{\sqrt{M}} \langle k | \sigma_y^- | K\nu \rangle \\ &= g_{K-k}^* \bar{\eta}_{\frac{K}{2}-k}^{(K\nu)}, \end{aligned} \quad (29)$$

where the quantity $\bar{\eta}_{\frac{K}{2}-k}^{(K\nu)}$ (for details, we refer to Sec. E) can be interpreted as a collective dipole moment. This quantity (which will be discussed later in this Section) can be used to define the branching ratio $b_k^{(K\nu)}$ for the decay $|K\nu\rangle \rightarrow |k\rangle$ via

$$\begin{aligned} b_k^{(K\nu)} &\equiv \frac{|g_{K-k}|^2 \left| \bar{\eta}_{\frac{K}{2}-k}^{(K\nu)} \right|^2}{\sum_{q=-\frac{\pi}{a}}^{\frac{\pi}{a}} |g_{K-q}|^2 \left| \bar{\eta}_{\frac{K}{2}-q}^{(K\nu)} \right|^2} \\ &\simeq \frac{\left| \bar{\eta}_{\frac{K}{2}-k}^{(K\nu)} \right|^2}{\sum_{q=\frac{K}{2}-\frac{\pi}{a}}^{\frac{K}{2}+\frac{\pi}{a}} \left| \bar{\eta}_q^{(K\nu)} \right|^2} = \frac{1}{2} \cdot \left| \bar{\eta}_{\frac{K}{2}-k}^{(K\nu)} \right|^2. \end{aligned} \quad (30)$$

In the second last step, we have exploited that the coupling strength is practically constant over the spectral range that corresponds to the wavenumbers involved. Also note that $\sum_q \left| \bar{\eta}_q^{(K\nu)} \right|^2 = 2$ holds (see Sec. E), which results from the branching ratio's sum over all decay channels $\sum_k b_k^{(K\nu)} = 1$. The partial rate for the decay $|K\nu\rangle \rightarrow |k\rangle$ is therefore

$$\Gamma_k^{K\nu} \equiv b_k^{K\nu} \cdot \Gamma_{\text{tot}}^{K\nu} = \frac{1}{2} \left| \bar{\eta}_{\frac{K}{2}-k}^{(K\nu)} \right|^2 \cdot \Gamma_{\text{tot}}^{K\nu}. \quad (31)$$

Hence, the collective dipole moment determines the branching ratio.

2. Momentum Distribution, Direct and Background Fluorescence

The quantity $\left| \bar{\eta}_q^{(K\nu)} \right|^2$ has yet another precise physical meaning. The Fourier transform of the two-body wave function (see Eq. (B3) for details), i.e.,

$$\begin{aligned} \sum_{n_1=-\frac{N}{2}}^{\frac{N}{2}} \sum_{n_2=-\frac{N}{2}}^{\frac{N}{2}} \frac{e^{-ik_1 an_1}}{\sqrt{M}} \frac{e^{-ik_2 an_2}}{\sqrt{M}} \Phi_{n_1 n_2} &= \\ \frac{1}{2M^{\frac{3}{2}}} \sum_{n_1=-\frac{N}{2}}^{\frac{N}{2}} \sum_{n_2=-\frac{N}{2}}^{\frac{N}{2}} e^{i(\frac{K}{2}-k_1)an_1} e^{i(\frac{K}{2}-k_2)an_2} \Psi_{n_1-n_2}^{(K\nu)} &= \\ \frac{1}{2} \bar{\eta}_{\frac{1}{2}(k_1-k_2)}^{(K\nu)} \delta_{[K-k_1-k_2] \frac{2\pi}{a}, 0}, \end{aligned} \quad (32)$$

demonstrates that $\left| \bar{\eta}_q^{(K\nu)} \right|^2$ can indeed be interpreted as the momentum distribution of the relative wave function with respect to a relative momentum q . The

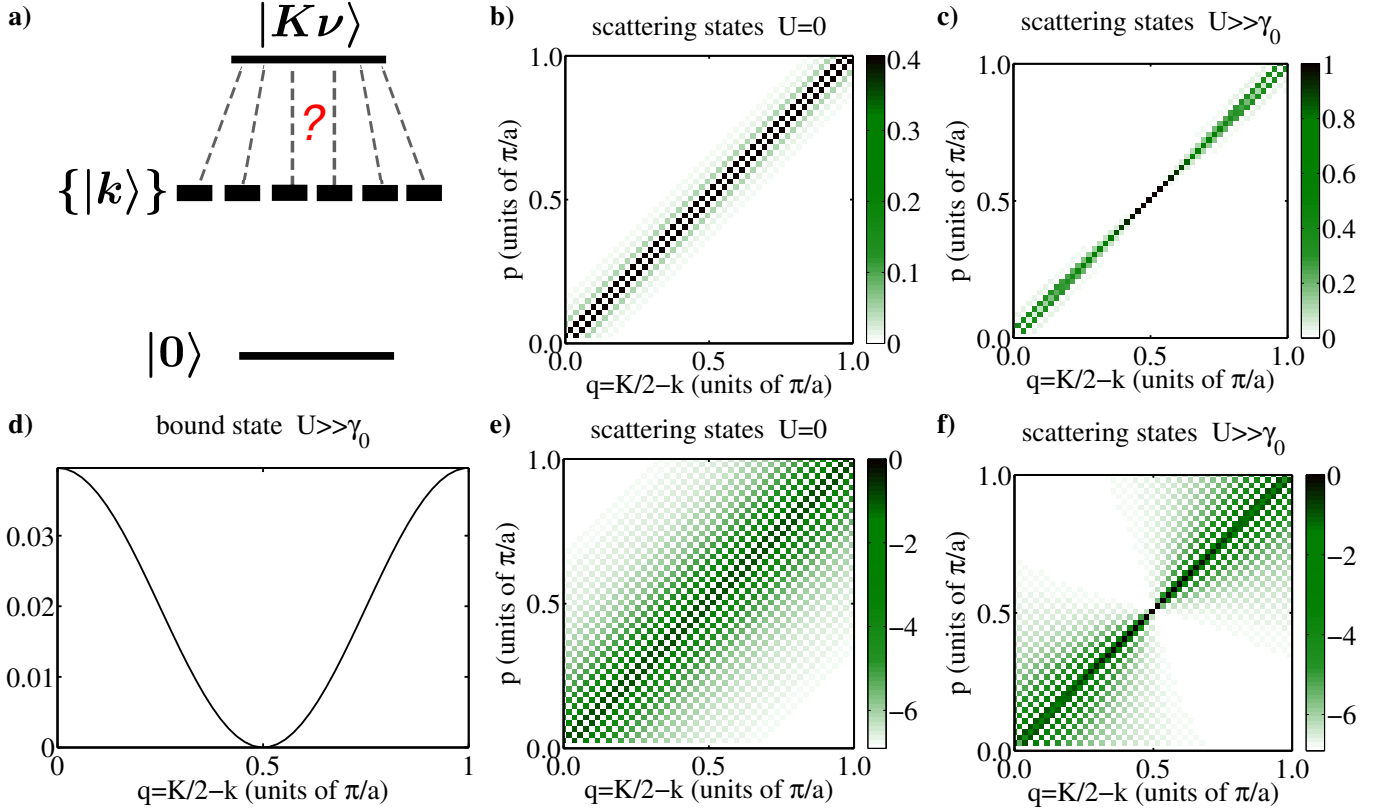


FIG. 3. (color online). a) How does a two-excitation state $|K\nu\rangle$ decay into the sub-manifold of single-excitation states $\{|k\rangle\}$? This can be answered with the help of the matrix elements of the collective dipole moment operator, which are intimately linked to the relative wavefunction's momentum distribution $|\bar{\eta}_q^{(K\nu)}|^2$. b) Momentum distribution $|\bar{\eta}_q^{(Kp)}|^2$ of the relative wavefunction for scattering states ($M = 101$) for $U = 0$ and c) $U \gg \gamma_0$. d) Momentum distribution $|\bar{\eta}_q^{(K,BS)}|^2$ of a bound state for $U \gg \gamma_0$ according to Eq. (37). e), f) Logarithmic plot of the scattering state's momentum distributions b) and c) (for better visualization, we have actually plotted $\ln(|\bar{\eta}_q^{(Kp)}|^2 + c)$ with $c = 10^{-3}$).

Kronecker- δ expresses the conservation of the center-of-mass wavenumber and the notation $[a]_b$ stands for “ a modulo b ”. As a result, the information about the individual decay paths of a two excitation eigenstate, i.e., collective dipole moments and branching ratios, are fully encoded in the momentum distribution of the eigenstate's relative wavefunction.

The explicit expressions are given as ($q \geq 0$ and $p > 0$, see App. E for details)

$$\bar{\eta}_q^{(Kp)} = \begin{cases} \frac{1+e^{i\delta_{Kp}}}{2} & p = q \\ \frac{2}{M} e^{i\frac{\delta_{Kp}}{2}} \frac{\sin[\frac{1}{2}(\delta_{Kp} - (p-q)a)]}{\sin[\frac{1}{2}(p-q)a]} & \left[\frac{(p-q)aM}{2\pi}\right]_2 \neq 0 \end{cases} \quad (33)$$

$$\bar{\eta}_q^{(K,BS)} = \frac{2}{\sqrt{M}} \cdot \frac{\cos(qa) - \alpha_K}{1 - 2\alpha_K \cos(qa) + \alpha_K^2}. \quad (34)$$

For the case of non-interacting atoms ($U = 0$), we have

$$|\bar{\eta}_q^{(K,p>0)}|^2 = \begin{cases} 0 & p = q \\ \frac{4}{M^2} \frac{1}{\tan^2[\frac{1}{2}(p-q)a]} & \left[\frac{(p-q)aM}{2\pi}\right]_2 \neq 0 \end{cases} \quad (35)$$

whereas in the regime of strong atom-atom interactions

($U \gg \gamma_0$) we are left with

$$|\bar{\eta}_q^{(K,p>0)}|^2 = \begin{cases} \sin^2(pa) & p = q \\ \frac{4}{M^2} \frac{1+\cos[(p+q)a]}{1-\cos[(p-q)a]} & \left[\frac{(p-q)aM}{2\pi}\right]_2 \neq 0 \end{cases} \quad (36)$$

$$|\bar{\eta}_q^{(K,BS)}|^2 = \frac{4}{M} \cos^2(qa). \quad (37)$$

Note that the symmetry properties $|\bar{\eta}_q^{(Kp)}|^2 = |\bar{\eta}_{-q}^{(Kp)}|^2$ and $|\bar{\eta}_q^{(Kp)}|^2 = |\bar{\eta}_q^{(K,-p)}|^2$ hold.

In Fig. 3b)–d), we plot the relative wavefunction's momentum distributions (35)–(37) on a linear scale. These figures reveal many details of the two-excitation states' properties and their respective decay channels. We start the discussion with a scattering state $|Kp\rangle$ for the case of non-interacting atoms ($U = 0$). Given the quantum numbers K and p , we can extract the values of $q = K/2 - k$ for which the momentum distribution is non-zero from Fig. 3b). This determines the wavenumbers $\{k\}$ of the intermediate single-excitation states that contribute to the overall decay $|Kp\rangle \rightarrow \{|k\rangle\} \rightarrow |0\rangle$. Since the main diagonal in Fig. 3b) is strictly zero, we can conclude that the decay channel with $\pm q = p$ is fully suppressed for

$U = 0$. Upon expressing the center-of-mass and relative wavenumbers in terms of single-excitation wavenumbers k_1 and k_2 (i.e., $K = k_1 + k_2$, $p = (k_1 - k_2)/2$), it becomes apparent that this “direct” channel with $\pm q = p$ (in the following also termed “direct fluorescence”) stands for decay processes where the intermediate single-excitation states are $|k_1\rangle$ and $|k_2\rangle$. In other words, the direct fluorescence refers to decay processes for which the single-excitation wavenumbers are individually conserved. This suppression which occurs for $U = 0$ is a consequence of the interaction-induced phase shift $e^{i\delta_{Kp}} = -1$ between the two excitations (see Eqs. (20) and (33)). Even though the atoms are non-interacting, the two excitations experience an infinitely strong on-site repulsion due to the hard-core constraint of spin-1/2 excitations ($\Psi_0^{(K\nu)} = 0$, see also Sec. II B 2), ultimately leading to the suppression of the direct channel. In addition to that, we have a “background” channel (also termed “background” fluorescence) for $\pm q \neq p$, yielding non-zero entries on the secondary diagonals in Fig. 3b) (see also Fig. 3e) for a logarithmic scale). The background fluorescence plays the dominant role for $U = 0$ and represents decay channels which do not conserve the individual single-excitation wavenumbers (the intermediate single-excitation states exhibit wavenumbers $k \neq k_1, k_2$).

Conversely, the details of a two-excitation scattering state’s decay in the regime $U \gg \gamma_0$ depend on the relative wavenumber p . From the relative wavefunction’s momentum distribution in Fig. 3c) (see also Fig. 3f) for a logarithmic scale), we infer that both direct and background fluorescence channels can occur. Specifically, at $p = \pi/2a$ the background channel is fully suppressed and only the direct fluorescence contributes. However, for relative wavenumbers away from $p = \pi/2a$, a combination of direct and background terms can be observed. Ultimately, close to $p = 0$ or $p = \pi/a$, the background fluorescence dominates and Fig. 3c) resembles Fig. 3b) (note the different scales). On the whole, the relative wavefunction’s momentum distribution for a scattering state in the regime $U \gg \gamma_0$ exhibits features as a function of the relative wavenumber p , whereas the regime of non-interacting atoms ($U = 0$) yields a featureless distribution (cf. Fig. 3b) and e)).

Finally, we discuss the respective momentum distribution of a bound state $|K, \text{BS}\rangle$ for $U \gg \gamma_0$. For a bound state, the concepts of “direct” and “background fluorescence” do not exist since the concept of a relative wavenumber p as a quantum number does not apply (a bound state is fully characterized by its center-of-mass wavenumber K). In Fig. 3d) we see that the momentum distribution is a broad function in momentum space (i.e., non-zero over a wide range of q). Hence, there are many intermediate single-excitation states to which a two-body bound state can decay. This property clearly contrasts a bound state from scattering states and will eventually lead to the characteristic and distinct features in the emission patterns which we discuss later.

D. Far-Field Observables

In this paper, we focus on the far-field signatures that emerge from the light that is scattered by the atoms. The Glauber decomposition of the electric field operator for the scattered far field can be written as [52, 53]

$$\hat{\mathbf{E}}^{(-)}(\mathbf{r}, t) = \xi \mathbf{w}(\mathbf{r}) \sum_n \sigma_n^+(t - t_n), \quad (38)$$

where $\xi = \omega_0^2/4\pi\epsilon_0 c^2$ (ϵ_0 is the vacuum permittivity),

$$\mathbf{w}(\mathbf{r}) = \frac{\mathbf{d}}{r} - (\mathbf{d} \cdot \mathbf{r}) \frac{\mathbf{r}}{r^3} \quad (r = |\mathbf{r}|) \quad (39)$$

signifies the far-field pattern of a single dipole, and $\hat{\mathbf{E}}^{(+)} = (\hat{\mathbf{E}}^{(-)})^\dagger$. The retarded times in the argument of the atomic operators in Eq. (38) are

$$t_n = \frac{1}{c} |\mathbf{r} - \mathbf{r}_n| = t_n(\beta_{\text{det}}) \quad (40)$$

$$\simeq \frac{r}{c} - \frac{a}{c} \sin(\beta_{\text{det}}) \cdot n, \quad (41)$$

where the last line represents the far-field approximation. Here, $\mathbf{r}_n = na\hat{\mathbf{z}}$ and β_{det} denotes the elevation coordinate of the detector position $\mathbf{r} = r(\cos \beta_{\text{det}} \cos \varphi_{\text{det}}, \cos \beta_{\text{det}} \sin \varphi_{\text{det}}, \sin \beta_{\text{det}})$ ($\beta_{\text{det}} = 0$ signifies detection perpendicular to the atomic chain and φ_{det} is the azimuthal angle).

We now transform to the basis of the system’s eigenstates by virtue of the expansion (for details, see App. C)

$$\begin{aligned} \sigma_n^- &= \sum_k |0\rangle \langle 0| \sigma_n^- |k\rangle \langle k| \\ &\quad + \sum_k \sum_{K\nu} |k\rangle \langle k| \sigma_n^- |K\nu\rangle \langle K\nu| \\ &= \frac{1}{\sqrt{M}} \sum_k e^{ikan} \hat{S}_{0;k} \\ &\quad + \frac{1}{2\sqrt{M}} \sum_k \sum_{K\nu} e^{i(K-k)an} \hat{\eta}_{\frac{K}{2}-k}^{(K,\nu)} \hat{S}_{k;K\nu}, \end{aligned} \quad (42)$$

where $\hat{S}_{0;k} = |0\rangle \langle k|$ and $\hat{S}_{k;K\nu} = |k\rangle \langle K\nu|$. The quantum number ν runs over all scattering states ($\nu = p$) and a possible bound state ($\nu = \text{BS}$). Assuming the “harmonic decomposition” [54] for the operators $\hat{S}_{0;k}$ and $\hat{S}_{k;K\nu}$, i.e.,

$$\hat{S}_{k;0}(t - t_n(\beta_{\text{det}})) \simeq e^{i\frac{\Delta_k^0}{c} a \sin \beta_{\text{det}} \cdot n} \hat{S}_{k;0}(t_{\text{ret}}), \quad (43)$$

$$\hat{S}_{K\nu;k}(t - t_n(\beta_{\text{det}})) \simeq e^{i\frac{\Delta_{K\nu}^k}{c} a \sin \beta_{\text{det}} \cdot n} \hat{S}_{K\nu;k}(t_{\text{ret}}) \quad (44)$$

(where $\Delta_k^{K\nu} \equiv \text{Re}(E_{K\nu}^{(2)} - E_k^{(1)})$ and $\Delta_0^k \equiv \text{Re}(E_k^{(1)})$ signify the transition energies and $t_{\text{ret}} \equiv t - r/c$ is the re-

tarded time), Eq. (38) turns into

$$\hat{\mathbf{E}}^{(-)}(\mathbf{r}, t) = \xi \mathbf{w}(\mathbf{r}) \sqrt{M} \times \sum_k \left(\delta_{k, [\Delta_0^k \sin(\beta_{\text{det}})/c]_{(2\pi/a)}} \hat{S}_{k;0}(t_{\text{ret}}) + \sum_{K\nu} \delta_{K-k, [\Delta_k^{K\nu} \sin(\beta_{\text{det}})/c]_{(2\pi/a)}} \left(\bar{\eta}_{\frac{K}{2}-k}^{(K\nu)} \right)^* \hat{S}_{K\nu;K}(t_{\text{ret}}) \right). \quad (45)$$

The Kronecker terms represent a constraint which relates the quantum numbers of a one-photon transition to the corresponding observation angle β_{det} via

$$k = \left[\frac{\Delta_0^k}{c} \sin \beta_{\text{det}} \right]_{\frac{2\pi}{a}}, \quad (46)$$

$$K - k = \left[\frac{\Delta_k^{K\nu}}{c} \sin \beta_{\text{det}} \right]_{\frac{2\pi}{a}}. \quad (47)$$

These expressions can be understood as specifying the wavenumbers that are transferred to the photon field under a given observation angle. Alternatively, for given K , ν , and/or k , we can determine the emission direction from these equations.

Since $\omega_0 \gg \gamma_0$, the Lamb shifts only yield a negligible wavenumber correction in Eqs. (46) and (47) and we can use the approximated expressions

$$k \simeq [k_{\text{at}} \sin \beta_{\text{det}}]_{\frac{2\pi}{a}}, \quad (48)$$

$$K - k \simeq [k_{\text{at}} \sin \beta_{\text{det}}]_{\frac{2\pi}{a}}. \quad (49)$$

To be precise, the decay of single-excitation states $|k\rangle \rightarrow |0\rangle$ requires $ka = 2\pi [(a/\lambda_{\text{at}}) \sin \beta_{\text{det}}]_1$, whereas for $|K\nu\rangle \rightarrow |k\rangle$ we have $(K - k)a = 2\pi [(a/\lambda_{\text{at}}) \sin \beta_{\text{det}}]_1$ (which is valid for both $U = 0$ and $\omega_0 \gg U \gg \gamma_0$). These expressions are reminiscent of Bragg's law and the emission angles are determined by matching the wave numbers transferred to the free-space photon field. For the remainder,

$$\bar{k} = \bar{k}(\mathbf{r}) = \bar{k}(\beta_{\text{det}}) = [k_{\text{at}} \sin \beta_{\text{det}}]_{\frac{2\pi}{a}} \quad (50)$$

denotes the wavenumber that can be detected at \mathbf{r} (which allows us to set $k = \bar{k}$ in the first and $k = K - \bar{k}$ in the second sum of Eq. (45), respectively). In terms of angles, we can rewrite this expression as

$$\sin \beta_{\text{det}} = \frac{\bar{k}}{k_{\text{at}}} + \frac{2\pi}{k_{\text{at}}a} \cdot n, \quad (51)$$

where $n = 0, \pm 1, \dots$ (such that $|\sin \beta_{\text{det}}| \leq 1$) signifies the Bragg order.

From Eq. (45), we can now construct arbitrary far-field observables. Specifically, the field-field auto-correlation function can be calculated from

$$\hat{G}^{(1)}(\mathbf{r}, t, t + \tau) \equiv \hat{\mathbf{E}}^{(-)}(\mathbf{r}, t) \hat{\mathbf{E}}^{(+)}(\mathbf{r}, t + \tau). \quad (52)$$

Evaluated at $\tau = 0$, we obtain the emitted intensity

$$\frac{\hat{G}^{(1)}(\mathbf{r}, t)}{\xi^2 |\mathbf{w}(\mathbf{r})|^2 M} = \hat{S}_{\bar{k};\bar{k}}(t_{\text{ret}}) + \sum_{K\nu\nu'} \bar{\eta}_{\frac{K}{2}-\bar{k}}^{(K\nu')} \left(\bar{\eta}_{\frac{K}{2}-\bar{k}}^{(K\nu)} \right)^* \hat{S}_{K\nu;K\nu'}(t_{\text{ret}}). \quad (53)$$

For a stationary state, the emission spectrum is defined as [55]

$$S(\mathbf{r}, \omega) = \lim_{t \rightarrow \infty} 2\text{Re} \left[\int_0^\infty d\tau e^{i\omega\tau} \langle \hat{G}^{(1)}(\mathbf{r}, t, t + \tau) \rangle \right] \quad (54)$$

where $\langle \dots \rangle$ denotes an expectation value. We employ the quantum regression theorem [53] for the calculation of the auto-correlation function's expectation value (see App. D for details).

Furthermore, the intensity correlation

$$\hat{G}^{(2)}(\mathbf{r}_1, \mathbf{r}_2) \equiv \hat{\mathbf{E}}^{(-)}(\mathbf{r}_1, t) \hat{G}^{(1)}(\mathbf{r}_2, t) \hat{\mathbf{E}}^{(+)}(\mathbf{r}_1, t) \quad (55)$$

for zero time-delay and two detector positions \mathbf{r}_1 and \mathbf{r}_2 can be obtained from

$$\frac{\hat{G}^{(2)}(\mathbf{r}_1, \mathbf{r}_2)}{\xi^4 |\mathbf{w}(\mathbf{r}_1)|^2 |\mathbf{w}(\mathbf{r}_2)|^2 M^2} = \sum_{\nu\nu'} \bar{\eta}_{\frac{1}{2}(k_1+k_2)}^{(k_1+k_2,\nu')} \left(\bar{\eta}_{\frac{1}{2}(k_1-k_2)}^{(k_1+k_2,\nu)} \right)^* \hat{S}_{k_1+k_2,\nu;k_1+k_2,\nu'}, \quad (56)$$

where k_1 and k_2 are the wavenumbers detected at \mathbf{r}_1 and \mathbf{r}_2 (elevation angles β_1 and β_2), respectively. The normalized intensity correlation

$$g^{(2)}(\mathbf{r}_1, \mathbf{r}_2) = g^{(2)}(\beta_1, \beta_2) = \frac{\langle \hat{G}^{(2)}(\mathbf{r}_1, \mathbf{r}_2) \rangle}{\langle \hat{G}^{(1)}(\mathbf{r}_1) \rangle \langle \hat{G}^{(1)}(\mathbf{r}_2) \rangle} \quad (57)$$

only depends on β_1 and β_2 and not on the details of the single-dipole patterns $|\mathbf{w}(\mathbf{r}_1)|^2$ and $|\mathbf{w}(\mathbf{r}_2)|^2$.

III. SPONTANEOUS EMISSION DYNAMICS

In this Section, we investigate the far-field signatures that emerge in the context of spontaneous decay, assuming the system has been prepared in a (pure) eigenstate at time $t = 0$.

A. Lindblad Equation

Based on the knowledge of the dissipative eigenstates, we formulate a Lindblad equation in order to account for the full dynamics that includes the decay from the two-excitation submanifold via the single-excitation subspace to the vacuum. To this end, we write the density matrix

as

$$\begin{aligned}
\hat{\varrho} = & \sum_{K\nu} \sum_{K'\nu'} \varrho_{K\nu;K'\nu'} |K\nu\rangle \langle K'\nu'| \\
& + \sum_{kk'} \varrho_{k;k'} |k\rangle \langle k'| + \varrho_{0;0} |0\rangle \langle 0| \\
& + \sum_{K\nu} \sum_k \varrho_{K\nu;k} |K\nu\rangle \langle k| + \text{h.c.} \\
& + \sum_{K\nu} \varrho_{K\nu;0} |K\nu\rangle \langle 0| + \text{h.c.} \\
& + \sum_k \varrho_{k;0} |k\rangle \langle 0| + \text{h.c.},
\end{aligned} \tag{58}$$

where we utilize the non-dissipative basis (formally realized by setting $\text{Re}(\Gamma_0) = \text{Re}(\Gamma_1) = 0$) as explained in the introduction of Sec. II B. The dynamics is governed by the Lindblad equation

$$\partial_t \hat{\varrho} = i[\hat{\varrho}, H'] + \mathcal{L}(\hat{\varrho}), \tag{59}$$

where

$$\begin{aligned}
H' = & \sum_{K\nu} \text{Re}(E_{K\nu}^{(2)}) \hat{S}_{K\nu;K\nu} + \sum_k \text{Re}(E_k^{(1)}) \hat{S}_{k;k}, \tag{60} \\
\mathcal{L}(\hat{\varrho}) = & \sum_{K\nu} \sum_k \left[R_{K\nu;k} \hat{\varrho} R_{K\nu;k}^\dagger - \frac{1}{2} \left\{ R_{K\nu;k}^\dagger R_{K\nu;k}, \hat{\varrho} \right\} \right] \\
& + \sum_k \left[R_{k;0} \hat{\varrho} R_{k;0}^\dagger - \frac{1}{2} \left\{ R_{k;0}^\dagger R_{k;0}, \hat{\varrho} \right\} \right]. \tag{61}
\end{aligned}$$

The dissipators are given as

$$R_{K\nu;k} \equiv \sqrt{\Gamma_k^{K\nu}} \hat{S}_{K\nu;k}, \tag{62}$$

$$R_{k;0} \equiv \sqrt{\Gamma_k} \hat{S}_{k;0}. \tag{63}$$

The curly brackets in Eq. (61) denote an anti-commutator.

The resulting equations of motion read

$$\partial_t \varrho_{K\nu;K'\nu'} = \left[-\frac{1}{2} (\Gamma_{\text{tot}}^{K\nu} + \Gamma_{\text{tot}}^{K'\nu'}) - i\Delta_{K'\nu'}^{K\nu} \right] \varrho_{K\nu;K'\nu'} \tag{64}$$

$$\begin{aligned}
\partial_t \varrho_{k;k'} = & \left[-\frac{1}{2} (\Gamma_k + \Gamma_{k'}) - i\Delta_{k'}^k \right] \varrho_{k;k'} \\
& + \delta_{k,k'} \sum_{K\nu} \Gamma_k^{K\nu} \varrho_{K\nu;K\nu},
\end{aligned} \tag{65}$$

$$\partial_t \varrho_{0;0} = \sum_k \Gamma_k \varrho_{k;k}, \tag{66}$$

$$\partial_t \varrho_{K\nu;k} = \left[-i\Delta_k^{K\nu} - \frac{1}{2} (\Gamma_{\text{tot}}^{K\nu} + \Gamma_k) \right] \varrho_{K\nu;k}, \tag{67}$$

$$\partial_t \varrho_{K\nu;0} = \left[-i\text{Re}(E_{K\nu}^{(2)}) - \frac{1}{2} \Gamma_{\text{tot}}^{K\nu} \right] \varrho_{K\nu;0}, \tag{68}$$

$$\partial_t \varrho_{k;0} = \left[-i\Delta_0^k - \frac{1}{2} \Gamma_k \right] \varrho_{k;0}, \tag{69}$$

where $\Delta_{K'\nu'}^{K\nu} \equiv \text{Re}(E_{K\nu}^{(2)} - E_{K'\nu'}^{(2)})$ and $\Delta_{k'}^k \equiv \text{Re}(E_k^{(1)} - E_{k'}^{(1)})$. The solution to this set of equations

is

$$\varrho_{K\nu;K'\nu'}(t) = e^{-i\Delta_{K'\nu'}^{K\nu} t} e^{-\frac{1}{2}(\Gamma_{\text{tot}}^{K\nu} + \Gamma_{\text{tot}}^{K'\nu'}) t} \varrho_{K\nu;K'\nu'}(0), \tag{70}$$

$$\begin{aligned}
\varrho_{k;k'}(t) = & \delta_{kk'} \sum_{K\nu} \frac{\Gamma_k^{K\nu}}{\Gamma_{\text{tot}}^{K\nu} - \Gamma_k} \left(e^{-\Gamma_k t} - e^{-\Gamma_{\text{tot}}^{K\nu} t} \right) \cdot \varrho_{K\nu;K\nu}(0) \\
& + e^{-i\Delta_{k'}^k t} e^{-\frac{1}{2}(\Gamma_k + \Gamma_{k'}) t} \varrho_{k;k'}(0),
\end{aligned} \tag{71}$$

$$\varrho_{0;0}(t) = 1 - \sum_{K\nu} \varrho_{K\nu;K\nu}(t) - \sum_k \varrho_{k;k}(t), \tag{72}$$

$$\varrho_{K\nu;k}(t) = e^{-i\Delta_k^{K\nu} t} e^{-\frac{1}{2}(\Gamma_{\text{tot}}^{K\nu} + \Gamma_k) t} \varrho_{K\nu;k}(0), \tag{73}$$

$$\varrho_{K\nu;0}(t) = e^{-i\text{Re}(E_{K\nu}^{(2)}) t} e^{-\frac{1}{2}\Gamma_{\text{tot}}^{K\nu} t} \varrho_{K\nu;0}(0), \tag{74}$$

$$\varrho_{k;0}(t) = e^{-i\Delta_0^k t} e^{-\frac{1}{2}\Gamma_k t} \varrho_{k;0}(0). \tag{75}$$

For the initial condition of a pure eigenstate, the coherences are zero at all times. In addition to that, for $\omega_0 \gg \gamma_0$, the above equations can be reduced to

$$\varrho_{K\nu;K\nu}(t) \simeq e^{-2\gamma_0 t} \varrho_{K\nu;K\nu}(0), \tag{76}$$

$$\begin{aligned}
\varrho_{k;k}(t) \simeq & \sum_{K\nu} 2b_k^{(K\nu)} (e^{-\gamma_0 t} - e^{-2\gamma_0 t}) \varrho_{K\nu;K\nu}(0) \\
& + e^{-\gamma_0 t} \varrho_{k;k}(0).
\end{aligned} \tag{77}$$

To be precise, for an initial single-excitation state, i.e., $\varrho_{k;k}(0) = 1$ (for a single k), we simply find

$$\varrho_{k;k}(t) \simeq e^{-\gamma_0 t}. \tag{78}$$

Similarly, for an initial two-excitation state ($\varrho_{K\nu;K\nu}(0) = 1$), the dynamics is

$$\varrho_{K\nu;K\nu}(t) \simeq e^{-2\gamma_0 t}, \tag{79}$$

$$\begin{aligned}
\varrho_{k;k}(t) \simeq & 2b_k^{(K\nu)} (e^{-\gamma_0 t} - e^{-2\gamma_0 t}) \\
& = \left| \bar{\eta}_{\frac{K}{2}-k}^{(K\nu)} \right|^2 (e^{-\gamma_0 t} - e^{-2\gamma_0 t}).
\end{aligned} \tag{80}$$

In the next Section, we answer the question of how this “internal” dynamics of the atomic system translates to signatures that can be detected in the optical far field.

B. Emitted Intensity

The intensity which is emitted by an initial eigenstate and detected in the far field can be obtained from the expectation value of Eq. (53) via $G^{(1)}(\mathbf{r}, t) \equiv \langle \hat{G}^{(1)}(\mathbf{r}, t) \rangle = \text{tr}[\hat{G}^{(1)} \hat{\varrho}]$, i.e.,

$$\frac{G^{(1)}(\mathbf{r}, t)}{\xi^2 |\mathbf{w}(\mathbf{r})|^2 M} = \varrho_{\bar{k};\bar{k}}(t_{\text{ret}}) + \left| \bar{\eta}_{\frac{K}{2}-\bar{k}}^{(K\nu)} \right|^2 \varrho_{K\nu;K\nu}(t_{\text{ret}}). \tag{81}$$

According to Eq. (78), an initial single-excitation state $|k\rangle$ yields the far-field intensity

$$\frac{G^{(1)}(\mathbf{r}, t)}{\xi^2 |\mathbf{w}(\mathbf{r})|^2 M} = e^{-\gamma_0 t_{\text{ret}}} \delta_{k, [k_{\text{at}} \sin \theta_{\text{det}}]_{(2\pi/a)}}, \tag{82}$$

which can be observed for elevation angles (see also Eq. (51))

$$\sin \beta_{\text{det}} = \frac{k}{k_{\text{at}}} + \frac{2\pi}{k_{\text{at}}a} \cdot n. \quad (83)$$

The spontaneous decay of a two-excitation state $|K\nu\rangle$ according to Eqs. (79) and (80) results in

$$\begin{aligned} \frac{G^{(1)}(\mathbf{r}, t)}{\xi^2 |\mathbf{w}(\mathbf{r})|^2 M} &= \left| \bar{\eta}_{\frac{K}{2}-\bar{k}}^{(K\nu)} \right|^2 (e^{-\gamma_0 t} - e^{-2\gamma_0 t}) + \left| \bar{\eta}_{\frac{K}{2}-\bar{k}}^{(K\nu)} \right|^2 e^{-2\gamma_0 t} \\ &= \left| \bar{\eta}_{\frac{K}{2}-\bar{k}}^{(K\nu)} \right|^2 e^{-\gamma_0 t_{\text{ret}}}, \end{aligned} \quad (84)$$

which is mono-exponential even though the overall decay is a two-step process ($|K\nu\rangle \rightarrow |\bar{k}\rangle \rightarrow |0\rangle$). Hence, we observe a mono-exponential decay at a rate γ_0 for scattering states ($\nu = p$), bound states ($\nu = \text{BS}$), as well as for single-excitation states (Eq. (82)). In other words, the temporal decay as such cannot serve as a characteristic fingerprint for identifying a specific state.

We therefore now turn to the discussion of the angle dependent emission pattern. According to Eq. (84), the far-field intensity as a function of the detection angle β_{det} normalized to the single-dipole pattern and the atom number (and, for simplicity, evaluated at a fixed time $t_{\text{ret}} = 0$) is completely determined by the momentum distribution of the eigenstate's relative wavefunction. In other words, the quantity $G^{(1)}(\mathbf{r}(\beta_{\text{det}}))/\xi^2 |\mathbf{w}(\mathbf{r}(\beta_{\text{det}}))|^2 M$ is in principle just another way of plotting the momentum distribution $|\bar{\eta}_{K/2-\bar{k}}^{(K\nu)}|^2$. Hence, Figs. 3 already contain the information about the emission pattern but we have to analyze this information as a function of the detection angle β_{det} (rather than as a function of $q = K/2 - \bar{k}$).

1. Emission Pattern of Scattering States

In Fig. 4, we depict the normalized emission pattern emerging from the decay of an initial scattering state $|K = 0, p\rangle$ for the two cases $U = 0$ and $U \gg \gamma_0$ and for different relative wavenumbers p . We visualize this pattern as a function of the detection angle β_{det} and use the emission wavelength λ_{at} (in units of a) as a parameter.

Similarly to Sec. II C 2, we begin the discussion with the case of non-interacting atoms ($U = 0$, a)–c) in Fig. 4. We notice that the “middle regions” of the emission peaks are zero. This is a consequence of the background fluorescence which is the relevant decay mechanism for $U = 0$. These “dark” middle regions (which are surrounded by non-zero contributions) correspond to the direct channel (i.e., the case $\pm q = p$ in Sec. II C 2) which is completely suppressed for $U = 0$. This observation is unique to all relative wavenumbers p for $U = 0$ (Fig. 4a)–c)) since the momentum distributions in the case of non-interacting atoms are featureless with respect to the relative wavenumber (see the discussion in Sec. II C 2). In contrast to this, for $U \gg \gamma_0$, we found that the momentum

distributions can be qualitatively different for different relative wavenumbers since a combination of background and direct fluorescence can occur. These properties manifest themselves in the emission patterns as depicted in Fig. 4d)–f). For $p = \pi/2a$ (Fig. 4d)), we observe single peaks as a function of the emission angle. This is a direct consequence of the fact that the momentum distribution for $p = \pi/2a$ in the regime $U \gg \gamma_0$ exclusively exhibits the direct channel as an allowed decay mechanism. Hence, we observe emission peaks at exactly those angles which would correspond to the aforementioned “dark” middle regions for $U = 0$. However, as we choose relative wavenumbers away from $p = \pi/2a$ (e.g., $p = \pi/4a$ in Fig. 4e) and $p = \pi/8a$ in Fig. 4f)), light emitted via background fluorescence becomes important. Especially in Fig. 4f), we can see that for $p = \pi/8a$ the emission pattern almost looks as in the case of non-interacting atoms (Fig. 4c)), except for the “middle region” of the emission peaks that stems from some remaining contribution of the direct fluorescence. The relative intensities between direct and background fluorescence can be inferred from the corresponding momentum distributions in Figs. 3b) and c).

Based on Eq. (51) we can also discuss the case where the bare atomic emission wavelength is much larger than the distance between the atoms, i.e., $\lambda_{\text{at}}/a \rightarrow \infty$, as well as the case of an isolated atom ($\lambda_{\text{at}}/a \rightarrow 0$). However, one should keep in mind that our tight-binding model becomes invalid when $\lambda_{\text{at}}/a \rightarrow \infty$ and one would have to sum up all dipole–dipole coupling terms for the eigenproblem in Sec. II B (not just the coupling to nearest neighbors). From Eq. (51) we can deduce that, in the limit $\lambda_{\text{at}}/a \rightarrow \infty$, the emission angles can only remain real-valued for $n = 0$, which means that only a single Bragg order would be observable. In contrast to this, the opposite limit of an isolated atom ($\lambda_{\text{at}}/a \rightarrow 0$) results in a continuum of possible emission angles as infinitely many Bragg orders are allowed.

Finally, we utilize Fig. 5 to conclude the discussion with some remarks on the width of the emission peaks. Remember that the wavenumber spacing is $\delta k \equiv 2\pi/aM$. Since the allowed wavenumbers are discrete, the resulting emission angles are also discrete. As an estimation for the resulting spacing of the detection angles, we can employ Eq. (49) and assume two transferred wavenumbers differing by δk , resulting in an angle difference of $\delta\beta_{\text{det}} \sim \delta k/k_{\text{at}} = \lambda_{\text{at}}/aM$. However, in the limit of many atoms, the angles become infinitely sharp. Hence, also the aforementioned “middle region” associated to the background fluorescence becomes infinitesimally small. Figure 5 illustrates how the spacing of the discrete emission angles affects the emission pattern of an initial scattering state $|K = 0, p = \pi/2a\rangle$ as the number of atoms M increases. As before, we have chosen the value of $p = \pi/2a$ for the relative wavenumber in Fig. 5 to highlight the differences between the background and direct fluorescence channels for $U = 0$ and $U \gg \gamma_0$, respectively. For instance, note how the “middle region” of the emis-

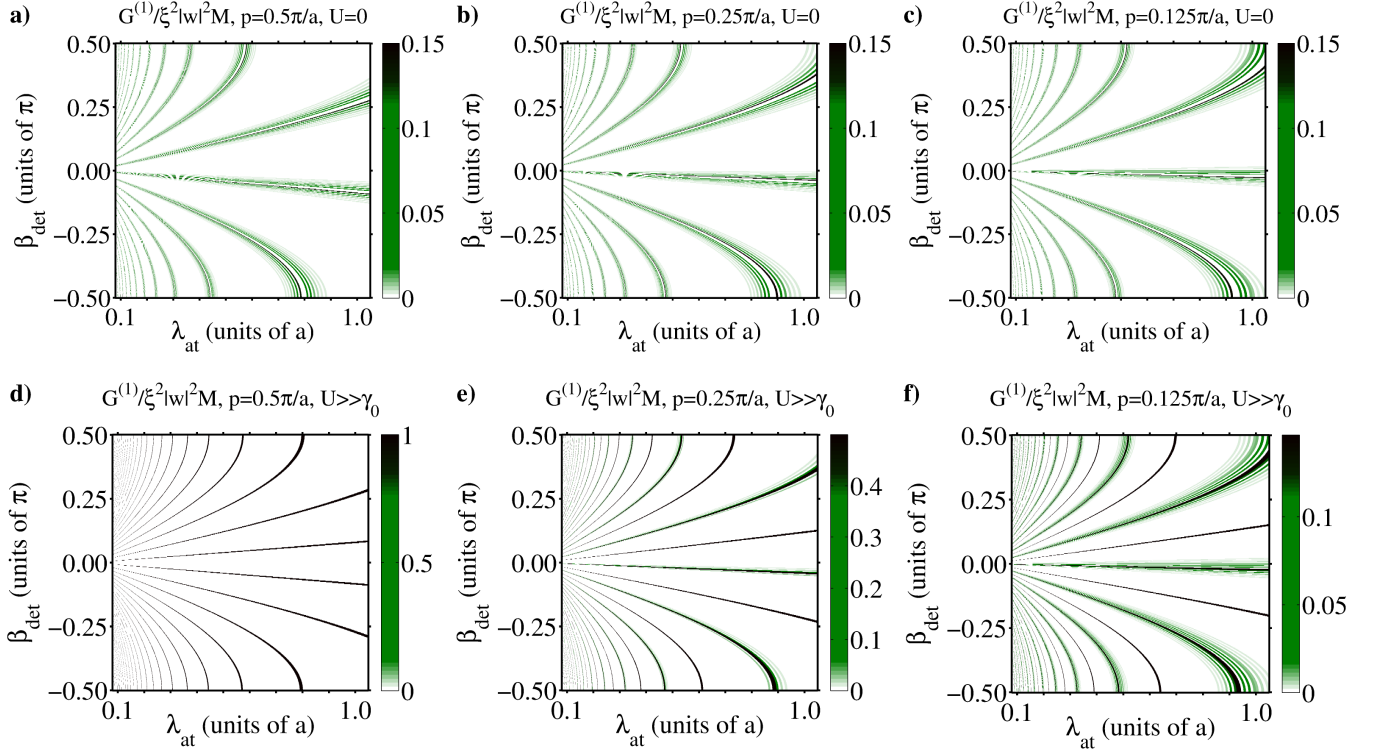


FIG. 4. (color online). Spontaneous emission patterns according to Eq. (84) for an initial state $|K = 0, p\rangle$ as a function of the detection angle β_{det} and the emission wavelength λ_{at} in units of a ($M = 101$). Top row: $U = 0$, bottom row: $U \gg \gamma_0$. From left to right: $pa/\pi = 1/2, 1/4, 1/8$. Note the different scales of the colorbars.

sion peaks for $U = 0$ becomes smaller as M increases.

2. Emission Pattern of Bound States

For a bound state $|K, \text{BS}\rangle$ in the presence of strong atom-atom interactions $U \gg \gamma_0$, the far-field intensity can be written as (cf. Eqs. (37) and (84))

$$\frac{G^{(1)}(\mathbf{r}, t)}{\xi^2 |\mathbf{w}(\mathbf{r})|^2} = 4 \cos^2 \left(\frac{Ka}{2} - \frac{2\pi a}{\lambda_{\text{at}}} [\sin \beta_{\text{det}}] \frac{\lambda_{\text{at}}}{a} \right) e^{-\gamma_0 t_{\text{ret}}}. \quad (85)$$

Note that this expression does not depend on the number of atoms M , which can be interpreted as a consequence of the bound state being spatially localized (rather than delocalized which would cover all atoms).

Figure 6 displays the bound state's emission pattern, which can be regarded as a distinct feature for proving the existence of a bound state on the lattice. The bound state sets a minimal spatial scale given by the relative wavefunction's spatial extent. For $U \gg \gamma_0$, this is simply the lattice constant a . Therefore, the momentum distribution covers a finite window in momentum space (on the order of $\delta k \sim 2\pi/a$), which translates into emission peaks having a finite width $\delta\beta_{\text{det}} \sim \lambda_{\text{at}}/a$. This width is independent of the number of atoms M and it is larger than the emission angle spacing due to a finite

lattice (see discussion in the context of scattering states). This property is in stark contrast to the sharp peaks that would be observed for delocalized single-excitation states or for two-excitation scattering states. In Fig. 7, we additionally display the influence of the strength of the atom-atom interaction U , where we utilize Eq. (84) together with Eq. (34). Already moderate values of U/γ_0 realize the result we obtained for $U \gg \gamma_0$ (e.g., see $U/\gamma_0 = 5$ in Fig. 7), justifying our previous assumptions. Note that Fig. 7a) depicts the special situation where the criterion (26) for the existence of a bound state is not fulfilled for certain of the shown values of λ_{at}/a . Consequently, no light emission from a bound state can be observed in these regions which are “dark” across all detection angles β_{det} . For $K = 0$ and $U > 0$ criterion (26) simply reads $|\text{Im}(\Gamma_1)| < U$. Since the quantity $\text{Im}(\Gamma_1)$ displays an oscillatory behavior as a function of $k_{\text{at}}a = 2\pi a/\lambda_{\text{at}}$ (cf. Eqs. (4)–(8)), a “bright” region in between two “dark” regions can be observed (as a function of λ_{at}/a) in Fig. 7a).

In conclusion, the angle-dependent far-field spontaneous emission pattern provides a distinct signature for identifying and studying the individual single- and two-excitation eigenstates. Moreover, without the need to address and/or manipulate single atoms, we gain access to the relative wavefunction's complete momentum distribution (see also Eq. (84)). This is achieved by tuning

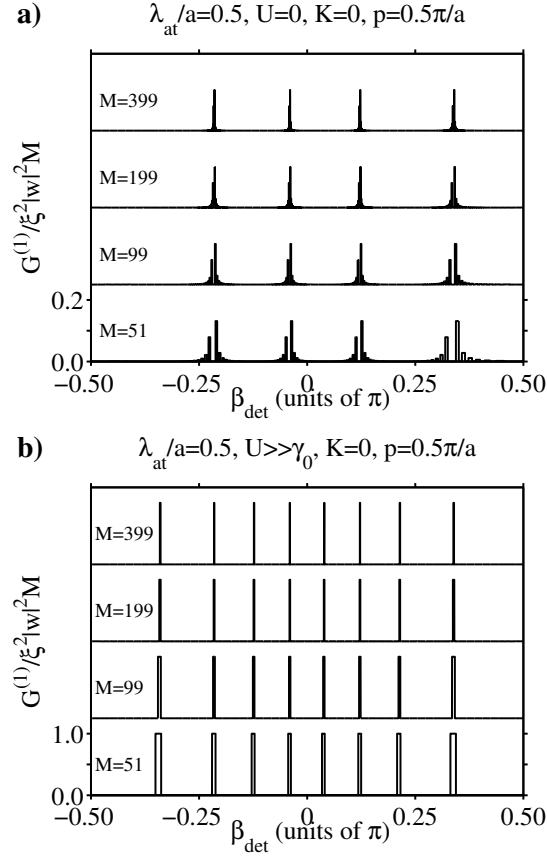


FIG. 5. Spontaneous emission patterns as in Fig. 4 for an initial scattering state $|K = 0, p = \pi/2a\rangle$ but for a fixed value of the emission wavelength $\lambda_{\text{at}}/a = 0.5$. In essence, this figure represents a cut of Figs. 4a) and d) along $\lambda_{\text{at}}/a = 0.5$. We have plotted the angle-dependent emission pattern for various atom numbers $M = 51, 99, 199, 399$. Note that the x -axis is discrete and that we have plotted each data point with a width $\delta\beta_{\text{det}}(M)$ with respect to the x -axis.

the argument $q = K/2 - \bar{k}(\beta_{\text{det}})$ across the first Brillouin zone. Given a value for K , this means we would need to sweep over the detection angles β_{det} for realizing different values of $\bar{k} = [k_{\text{at}} \sin \beta_{\text{det}}]_{2\pi/a}$.

IV. STEADY-STATE SIGNATURES UNDER THE INFLUENCE OF A WEAK DRIVING FIELD

All considerations in Sec. III assumed the system to be prepared in a pure eigenstate at time $t = 0$ and the far-field intensity discussed is a consequence of the system's evolution in the absence of external driving fields. The pulsed excitation of x-ray quantum optical systems [25] already approximately realizes these conditions. For example, in the archetype setup of ^{57}Fe Mössbauer nuclei driven by synchrotron radiation, the exciting synchrotron pulse has a duration of order 10-100ps, whereas the natural lifetime of the nuclei is about 140ns. Our study is

of high significance for this field, since state-of-the-art experiments operate in the single-excitation regime, and have the capability of probing individual eigenstates via a delicate choice of the sample geometry [36, 38, 39, 42]. It would be highly desirable to make the double-excitation states studied in our paper accessible to those experiments. However, since such constraints may be difficult with regard to experimental realizations in general, we now turn to the discussion of the system's response to an external driving field. In particular, we focus on the steady state that emerges when the system is probed optically in a very simple way.

A. Rate Equations

Specifically, we consider a weak (i. e., strongly attenuated) incoherent driving field (e. g., pseudothermal light [56]) with a spatial plane-wave pattern. Choosing the external field to be incoherent greatly simplifies the theoretical description as we can resort to a set of rate equations rather than solving the master equation with all coherences (see Eqs. (87) and (88) below). Let $|\mathcal{P}_n|^2$ be the pump rate of the driving field's n -th plane wave component whose spatial projection on the direction of the atomic chain is of the form $\exp(ik_n^{(z)}z)$, where $k_n^{(z)}$ signifies the z -component of the driving field's wavevector \mathbf{k}_n (magnitude $|\mathbf{k}_n| = k_L = k_{\text{at}} = 2\pi/\lambda_{\text{at}}$). This external wavenumber “imprints” the “internal” wavenumber

$$k_n = \left[k_n^{(z)} \right]_{\frac{2\pi}{a}} = \left[k_L \sin \beta_{\text{exc}}^{(n)} \right]_{\frac{2\pi}{a}} \quad (86)$$

on the atomic system, where $\beta_{\text{exc}}^{(n)}$ signifies the excitation angle ($\mathbf{k}^{(n)} = k_L(\cos \beta_{\text{exc}}^{(n)}, 0, \sin \beta_{\text{exc}}^{(n)})$, see also Fig. 1b)). A weak drive with $|\mathcal{P}_n|^2 \ll \gamma_0$ allows us to work in the truncated Hilbert space of at most two excitations. Note that in practice the pump rates actually depend on the external field's angle of incidence since ultimately the projection of the pump's linearly polarized electric field on the atomic dipole moments is of relevance. There is especially no coupling for angles where the dipole moment and the electric field are perpendicular to each other. In the following, this specific dependence of the pump rate on the angle of incidence will not be taken into account explicitly. Rather, we assume the external field's parameters to be tunable such that the pump rate is adjusted for each angle and we effectively get angle-independent driving terms.

We can then extend Eqs. (64)–(69) to account for the external driving field, ultimately yielding a set of coupled rate equations for the diagonal elements $N_m \equiv \varrho_{m;m}$ of the density matrix. The steady state can be determined through (see App. F for details)

$$N_{K\nu} = \sum_n \frac{|\mathcal{P}_n|^2}{\Gamma_{\text{tot}}^{K\nu}} \left| \bar{\eta}_{\frac{K}{2}-k_n}^{(K,\nu)} \right|^2 N_{K-k_n}, \quad (87)$$

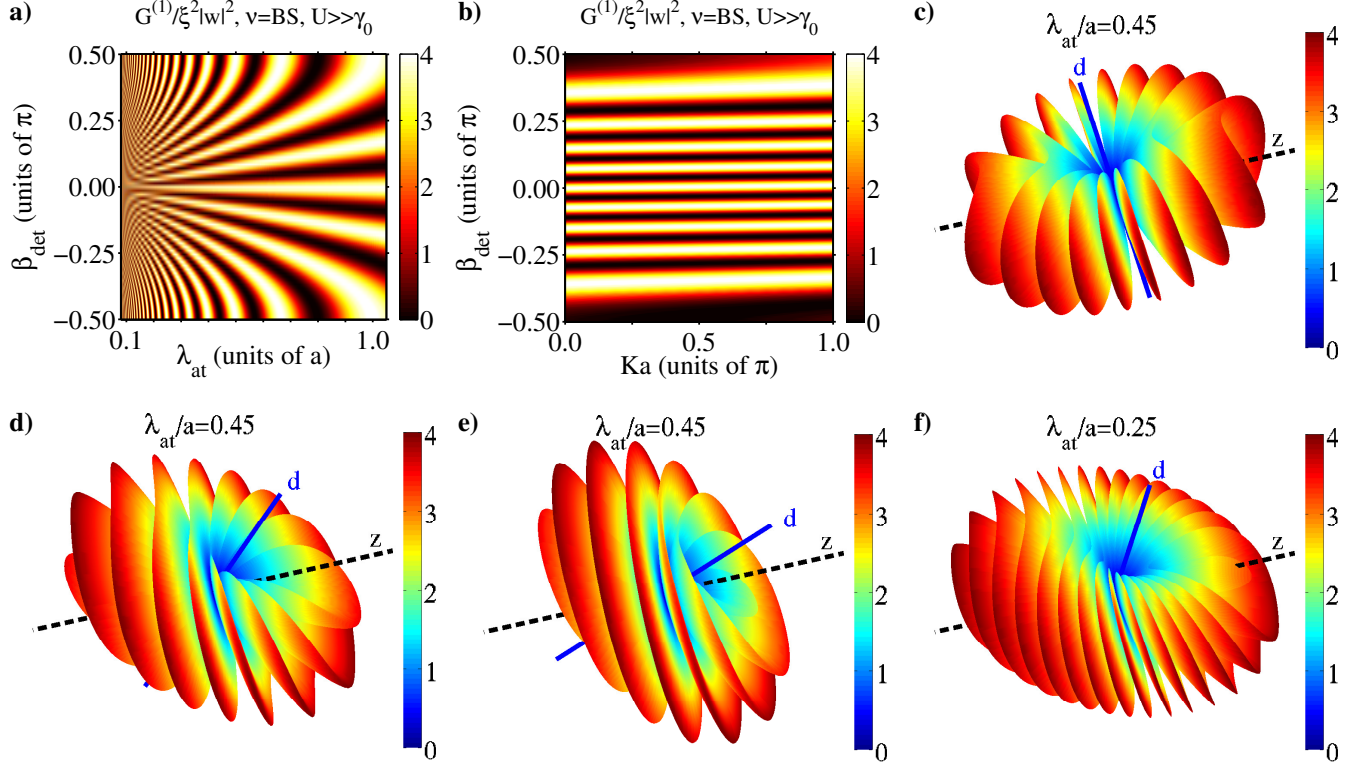


FIG. 6. (color online). Spontaneous emission patterns according to Eq. (85) (for $t_{\text{ret}} = 0$) emerging from an initial bound state $|K, \text{BS}\rangle$. a) Emission pattern (for $K = 0$) normalized to the single-dipole pattern as a function of the detection angle β_{det} and the emission wavelength λ_{at} (in units of a). As λ_{at}/a increases, less Bragg orders become visible and the width of the emission peaks increases. b) Emission pattern as in a) but for $\lambda_{\text{at}}/a = 0.45$ as a function of the detection angle and the center-of-mass wavenumber K . The full emission pattern taking into account the single-dipole pattern is shown in c)–f) (we have plotted $G^{(1)}r^2/\xi^2|d|^2$ for $K = 0$ as a 3D spherical plot, the colorbar indicates the emission strength). The patterns exhibit a toroidal-like structure (which is a remnant of the single-dipole pattern) with lobes resulting from the properties of the bound state’s momentum distribution. The angle between the single-atom dipole moment \mathbf{d} (denoted by the blue line) and the atomic chain (dashed black line) is c) $\theta = \pi/2$, d) $\theta = \pi/4$, e) $\theta = \pi/8$, and f) $\theta = \pi/3$.

$$N_k = \sum_n \frac{|\mathcal{P}_n|^2}{\tilde{\Gamma}_k} \delta_{kk_n} \left(1 - \sum_k N_k - \sum_{K\nu} N_{K\nu} \right) + \sum_{K\nu} \frac{\Gamma_k^{K\nu}}{\tilde{\Gamma}_k} N_{K\nu}. \quad (88)$$

We begin with the investigation of the atomic system’s steady state that emerges for the simple case where the external field exhibits only a single spatial Fourier component. In other words, we investigate the system’s response to a single external pump.

B. Single-Pump Setup

We envision an external driving field with a single spatial Fourier component which “imprints” the wavenumber $k_P = [k_L \sin \beta_{\text{exc}}^{(n)}]_{2\pi/a}$ on the atomic system (see Figs. 1b) and 8). The pump rate is $|\mathcal{P}|^2$ and for a weak pump we have $\Xi \equiv |\mathcal{P}|^2/\gamma_0 \ll 1$. The steady-state occupation numbers according to Eqs. (87) and (88) are (see

App. F 1 for details)

$$N_k \simeq \Xi \delta_{kk_P} + \Xi^2 \sum_{\nu} b_k^{(2k_P, \nu)} \left| \bar{\eta}_0^{(2k_P, \nu)} \right|^2 \quad (89)$$

$$= \Xi \delta_{kk_P} + \frac{\Xi^2}{2} \sum_{\nu} \left| \bar{\eta}_{k_P-k}^{(2k_P, \nu)} \right|^2 \left| \bar{\eta}_0^{(2k_P, \nu)} \right|^2,$$

$$N_{K\nu} \simeq \frac{\Xi^2}{2} \left| \bar{\eta}_0^{(2k_P, \nu)} \right|^2 \delta_{K, 2k_P}, \quad (90)$$

where we have assumed $\omega_0 \gg \gamma_0 \gg |\mathcal{P}|^2$. The external pump only directly drives single-excitation states $|k = k_P\rangle$ such that states $|k \neq k_P\rangle$ are populated via spontaneous emission of a two-excitation state $|K = 2k_P, \nu\rangle$, which is of order Ξ^2 . Furthermore, only two-excitation states with $K = 2k_P$ are excited (see Fig. 8).

Even though the pump only excites certain wavenumbers, the steady state that results from this simple, incoherent excitation scheme is still a mixed state. In the following, we analyze the signatures that emerge from

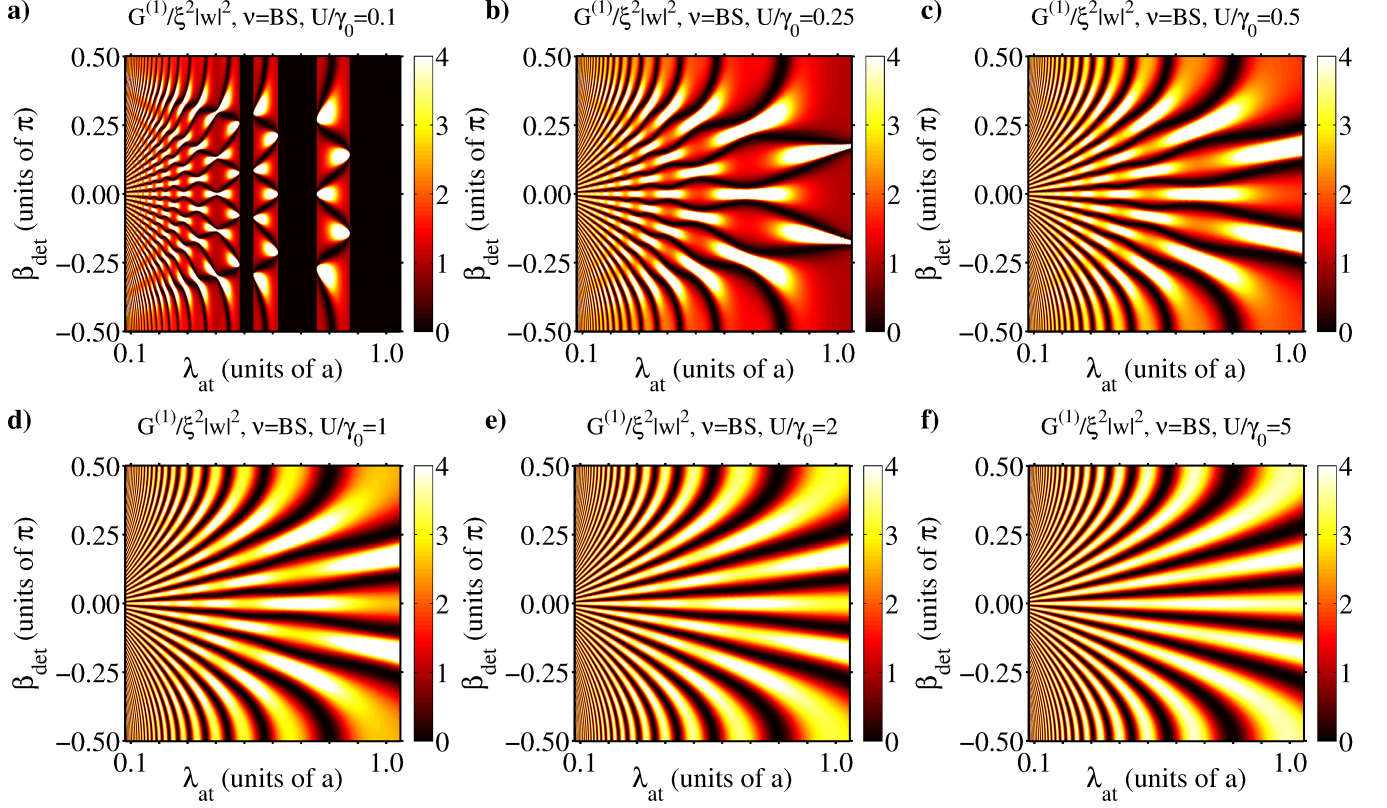


FIG. 7. (color online). Normalized emission pattern emerging from a bound state $|K = 0, \text{BS}\rangle$ as in Fig. 6, but for different strengths of the atom–atom interaction U (atomic dipole moments perpendicular to the atomic chain). Regions that are “dark” for any angle correspond to parameters for which the criterion for the existence of a bound state is not satisfied.

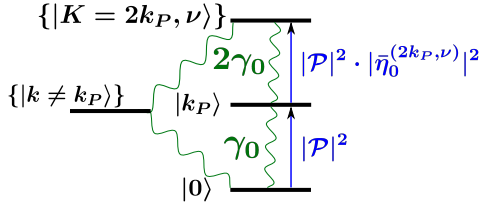


FIG. 8. Driving the 1D lattice of two-level atoms with an incoherent drive as sketched in Fig. 1b), reduces the Hilbert space to the levels shown here. Since the external pump “imprints” the wave number k_P on the atomic system the relevant Hilbert space comprises only two-excitation states with $K = 2k_P$.

this mixed state and investigate how they can be used for inferring information about the atomic system from the far field.

1. Far-Field Intensity

According to Eq. (53), the far-field intensity that emerges in the steady state is given by

$$\frac{G^{(1)}(\mathbf{r})}{\xi^2 |\mathbf{w}(\mathbf{r})|^2 M} = N_{\bar{k}} + \sum_{\nu} \left| \bar{\eta}_{k_P - \bar{k}}^{(2k_P, \nu)} \right|^2 N_{2k_P, \nu}, \quad (91)$$

where, as before, $\bar{k} = [k_{\text{at}} \sin \beta_{\text{det}}]_{2\pi/a}$ (and β_{det} is the elevation angle of the detector position \mathbf{r}). The intensity detected in the far field is thus always a sum of a contribution from a single-excitation state (first term), two-excitation scattering states, and a two-excitation bound state (if it exists). Upon insertion of the steady-state solutions (89)–(90), we arrive at

$$\frac{G^{(1)}(\mathbf{r})}{\xi^2 |\mathbf{w}(\mathbf{r})|^2 M} = \Xi \cdot \left(\delta_{\bar{k} k_P} + \Xi \sum_{\nu} \left| \bar{\eta}_{k_P - \bar{k}}^{(2k_P, \nu)} \right|^2 \left| \bar{\eta}_{k_P - \bar{k}}^{(2k_P, \nu)} \right|^2 \right). \quad (92)$$

A contribution that scales linearly with the pump power can only be observed for wavenumbers that match the wavenumber excited by the pump field ($\bar{k} = k_P$). Varying the pump-power would in principle allow to identify and separate the linear and quadratic terms in Eq. (92).

Performing the sum over ν in Eq. (92) (see App. G for

details) yields the explicit expression

$$\frac{G^{(1)}(\mathbf{r})}{\xi^2 |\mathbf{w}(\mathbf{r})|^2 M} = \Xi \delta_{\bar{k}k_P} \quad (93)$$

$$+ \Xi^2 \begin{cases} \frac{1}{3} \delta_{\bar{k}k_P} & \text{for } U = 0 \\ \frac{1}{3} \delta_{\bar{k}k_P} + \frac{16}{M^2} \cos^2 [(\bar{k} - k_P) a] & \text{for } U \gg \gamma_0 \end{cases}.$$

Hence, for detected wavenumbers that are different from the wavenumber enforced by the pump (i.e., $\bar{k} \neq k_P$), only light originating from the bound state contributes (see also App. G for details). However, this contribution is suppressed in the limit of many atoms $M \gg 1$ (scaling as $G^{(1)} \propto 1/M$). The only difference between the two cases $U = 0$ and $U \gg \gamma_0$ with respect to the far-field intensity for this single-pump setup is thus a small correction to the $M \gg 1$ -limit that comes from the bound state. Furthermore, the quantity (93) is a result of a sum over different states since the steady state is a mixed state. We therefore now turn to a frequency-specific far-field quantity—the emission spectrum.

2. Emission Spectrum

Using the definition (54), the emission spectrum reads (see App. D for details on the calculation of the field-field autocorrelation's expectation value via the quantum regression theorem)

$$\frac{S(\mathbf{r}, \omega) \gamma_0}{2\xi^2 |\mathbf{w}(\mathbf{r})|^2 M} = \quad (94)$$

$$\Xi \left[\frac{2}{\left(2 \frac{\omega - \omega_0}{\gamma_0}\right)^2 + 1} \left(\delta_{\bar{k}k_P} + \frac{\Xi}{2} \sum_{\nu} \left| \bar{\eta}_{k_P - \bar{k}}^{(2k_P, \nu)} \right|^2 \left| \bar{\eta}_0^{(2k_P, \nu)} \right|^2 \right) \right.$$

$$+ \frac{\Xi}{3} \frac{1}{\left(\frac{2}{3} \frac{\omega - \omega_0}{\gamma_0}\right)^2 + 1} \sum_p \left| \bar{\eta}_{k_P - \bar{k}}^{(2k_P, p)} \right|^2 \left| \bar{\eta}_0^{(2k_P, p)} \right|^2$$

$$\left. + \frac{\Xi}{3} \frac{1}{\left(\frac{2}{3} \frac{\omega - \omega_0 - U}{\gamma_0}\right)^2 + 1} \left| \bar{\eta}_{k_P - \bar{k}}^{(2k_P, \text{BS})} \right|^2 \left| \bar{\eta}_0^{(2k_P, \text{BS})} \right|^2 \right].$$

Again, the light emitted by the driven single-excitation state $|k_P\rangle$ scales linearly with the pump power ($\propto \Xi$), whereas all other contributions scale quadratically ($\propto \Xi^2$). Specifically, the contributions around $\omega = \omega_0$ (first and second Lorentzian) contain light from single-excitation states (first line) and two-excitation scattering states (see the sum over the relative wavenumber p in the second line). The contribution around $\omega = \omega_0 + U$ (third Lorentzian) is exclusively due to the bound state.

For $U = 0$, the last line in Eq. (94) would be absent. For $U \gg \gamma_0$, we can exploit the bound states' separation in energy from the band of scattering states (cf. Fig. 2). In other words, since $U \gg \gamma_0$, the corresponding emission spectrum at the frequency $\omega = \omega_0 + U$ has practically no overlap to transitions around $\omega = \omega_0$. We may then

extract the following information around the resonance $\omega = \omega_0 + U$:

$$\frac{S(\mathbf{r}, \omega = \omega_0 + U) \gamma_0}{2\xi^2 |\mathbf{w}(\mathbf{r})|^2 M} = \frac{\Xi^2}{3} \left| \bar{\eta}_{k_P - \bar{k}}^{(2k_P, \text{BS})} \right|^2 \left| \bar{\eta}_0^{(2k_P, \text{BS})} \right|^2 \quad (95)$$

$$= \frac{\Xi^2}{3} \cdot \frac{16}{M^2} \cos^2 [(\bar{k} - k_P) a].$$

When compared with Eq. (93), we see that this is the “pure” far-field signature for the existence of a two-body bound state on the lattice. Moreover, if we imagine the emission spectrum being measured at \mathbf{r} (elevation β_{det}) and, for convenience, normalize this signal to the value recorded at a fixed direction \mathbf{r}' ($|\mathbf{r}| = |\mathbf{r}'| = r$, elevation β_{exc}) in the y - z plane, we have

$$\frac{S(\mathbf{r}, \omega = \omega_0 + U)}{S(\mathbf{r}', \omega = \omega_0 + U)} \cdot \frac{|\mathbf{d}|^2 / r^2}{|\mathbf{w}(\mathbf{r})|^2} = \cos^2 [(k_P - \bar{k}) a] \quad (96)$$

$$= \cos^2 \left(k_P a - k_{\text{at}} a [\sin \beta_{\text{det}}] \frac{2\pi}{a} \right).$$

This is the same signature as obtained in the context of spontaneous emission from a pure eigenstate (see Eq. (85)), even though here the external probing field is incoherent and weak. The discussion from Sec. IIIB 2 therefore applies to this result as well. Hence, Eq. (96) does not only represent an explicit far-field feature for the existence of a bound state on a lattice. This expression can, analogous to the discussion of Eq. (85), be utilized to extract the relative wave function's complete momentum distribution by tuning the argument $k_P - \bar{k}$ across the first Brillouin zone. To this end, one could, for instance, vary the detection angle β_{det} while keeping the excitation angle β_{exc} fixed. The spectrum only needs to be recorded at a single frequency $\omega = \omega_0 + U$.

Conversely, around the frequency $\omega = \omega_0$ we can extract

$$\frac{S(\mathbf{r}, \omega = \omega_0) \gamma_0}{2\xi^2 |\mathbf{w}(\mathbf{r})|^2 M} = 2\Xi \delta_{\bar{k}k_P} + \frac{4}{3} \Xi^2 \sum_p \left| \bar{\eta}_{k_P - \bar{k}}^{(2k_P, p)} \right|^2 \left| \bar{\eta}_0^{(2k_P, p)} \right|^2$$

$$+ \Xi^2 \left| \bar{\eta}_{k_P - \bar{k}}^{(2k_P, \text{BS})} \right|^2 \left| \bar{\eta}_0^{(2k_P, \text{BS})} \right|^2, \quad (97)$$

which can be rewritten performing the sums over ν and p as (see App. G for details)

$$\frac{S(\mathbf{r}, \omega = \omega_0) \gamma_0}{2\xi^2 |\mathbf{w}(\mathbf{r})|^2 M} = 2\Xi \delta_{\bar{k}k_P} + \frac{4}{9} \Xi^2 \delta_{\bar{k}k_P}$$

$$+ \Xi^2 \begin{cases} 0 & \text{for } U = 0 \\ \frac{16}{M^2} \cos^2 [(\bar{k} - k_P) a] & \text{for } U \gg \gamma_0 \end{cases}. \quad (98)$$

Similar to the discussion of Eq. (93), the contribution from the bound state only appears for detected wavenumbers $\bar{k} \neq k_P$ as a correction to the $M \gg 1$ -limit. However, also here, we cannot infer more specific properties on the nature of the scattering states from the far field. This prompts for an extension of this simple single-pump excitation scheme to the case of an external field with two Fourier components.

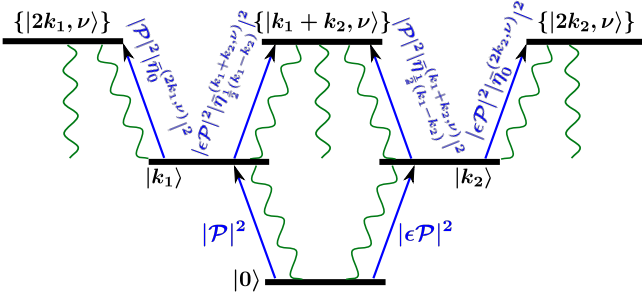


FIG. 9. An external, incoherent field with two spatial Fourier components (as depicted in Fig. 1c) drives the atomic system and “imprints” the wavenumbers k_1 and k_2 (the ratio of the driving fields’ pump rates is ϵ^2). The reduced level scheme for this two-pump excitation setup comprises single-excitation states $|k_1\rangle$ and $|k_2\rangle$, and two-excitation states $|2k_1, \nu\rangle$, $|2k_2, \nu\rangle$, and $|k_1 + k_2, \nu\rangle$. The figure shows the situation for the case $k_1 \neq k_2$. Single-excitation levels that are only populated via spontaneous emission from two-excitation states are not shown here since they would only be relevant for detection angles $\beta_{\text{det}}^{(1)} \neq \beta_1, \beta_2$ (which we do not consider).

C. Two-Pump Setup

In this Section, we investigate the atomic system’s far-field response along the same lines as in Sec. IV B but for a two-pump setup (see Fig. 1c)). We thus imagine two plane wave components with wavevectors $\mathbf{k}^{(1)}$ and $\mathbf{k}^{(2)}$, respectively ($|\mathbf{k}^{(1)}| = |\mathbf{k}^{(2)}| = k_L = k_{\text{atom}}$). The corresponding wavenumbers that are “imprinted” on the atomic system are $k_i = [k_{\text{atom}} \sin \beta_i]_{2\pi/a}$ ($i = 1, 2$), where β_i signify the excitation angles (angles of incidence). We choose the corresponding pump rates according to $|\mathcal{P}_1|^2 \equiv |\mathcal{P}|^2$ and $|\mathcal{P}_2|^2 \equiv \epsilon^2 |\mathcal{P}|^2$.

In Sec. IV B, we have revealed that the signatures at detection angles corresponding to wavenumbers that are not directly driven by the external pump (i.e., $\bar{k} \neq k_P$ in Sec. IV B, see also Fig. 8) only provide information about the bound state. Conversely, at detection angles corresponding to the wavenumber that is directly driven by the pump (i.e., $\bar{k} = k_P$ in Sec. IV B), the single-pump setup failed to provide specific details about the scattering states’ properties.

In the following, we will show how a two-pump setup can be exploited to gain further insight. To this end, we will, unlike in Sec. IV B, exclusively focus on an out-of-plane detection scheme where the detection angles coincide with the excitation angles, i.e., $\beta_{\text{det}}^{(i)} = \beta_i$. This choice considerably simplifies the relevant expressions for the steady-state occupation numbers (which can be found in App. F 2). Furthermore, it allows us to only consider those wavenumbers in the description that are imposed by the external field (i.e., $\bar{k}_i = k_i$).

1. Far-Field Intensity

The far-field intensity measured at a detector position \mathbf{r}_1 out-of-plane (elevation β_1 , detected wavenumber k_1) can be determined from Eq. (53), yielding

$$\frac{G^{(1)}(\mathbf{r}_1)}{\xi^2 |\mathbf{w}(\mathbf{r}_1)|^2 M} = N_{k_1} + \sum_{\nu} \left| \bar{\eta}_0^{(2k_1, \nu)} \right|^2 N_{2k_1, \nu} \quad (99)$$

$$+ (1 - \delta_{k_1 k_2}) \sum_{\nu} \left| \bar{\eta}_{\frac{1}{2}(k_1 - k_2)}^{(k_1 + k_2, \nu)} \right|^2 N_{k_1 + k_2, \nu}.$$

Inserting the steady-state occupation numbers (F32)–(F38) leads to

$$\frac{G^{(1)}(\mathbf{r}_1)}{\xi^2 |\mathbf{w}(\mathbf{r}_1)|^2 M} = \Xi (1 + \epsilon^2 \delta_{k_1 k_2}) \quad (100)$$

$$+ \Xi^2 \sum_{\nu} \left| \bar{\eta}_0^{(2k_1, \nu)} \right|^4 + 2\epsilon^2 \Xi^2 \sum_{\nu} \left| \bar{\eta}_{\frac{1}{2}(k_1 - k_2)}^{(k_1 + k_2, \nu)} \right|^4$$

$$+ \epsilon^4 \frac{\Xi^2}{2} (1 + \delta_{k_1 k_2}) \sum_{\nu} \left| \bar{\eta}_{k_2 - k_1}^{(2k_2, \nu)} \right|^2 \left| \bar{\eta}_0^{(2k_2, \nu)} \right|^2.$$

For $\epsilon = 0$ (i.e., zero second field) we simply recover Eq. (92) (for the case $\bar{k} = k_P$).

Note that Eq. (100) contains linear and non-linear terms in the dimensionless pump power Ξ . In order to investigate the dependence on the parameters that can be tuned externally, i.e., β_1 , β_2 , and ϵ , we start from the quantity

$$\bar{G}_{\text{NL}}^{(1)}(\beta_1, \beta_2, \epsilon) = \left[\frac{G^{(1)}(\mathbf{r}_1)}{\xi^2 |\mathbf{w}(\mathbf{r}_1)|^2 M} - \Xi (1 + \epsilon^2 \delta_{k_1 k_2}) \right] \cdot \frac{1}{\Xi}, \quad (101)$$

which is the rescaled, nonlinear part of the emitted intensity (low-power limit subtracted). In particular, we focus on the relative difference of this quantity for zero and non-zero second driving field. In other words, we define

$$\delta \bar{G}_{\text{NL}}^{(1)}(\beta_1, \beta_2, \epsilon) \equiv \frac{\bar{G}_{\text{NL}}^{(1)}(\beta_1, \beta_2, \epsilon) - \bar{G}_{\text{NL}}^{(1)}(\beta_1, \beta_2, \epsilon = 0)}{\bar{G}_{\text{NL}}^{(1)}(\beta_1, \beta_2, \epsilon = 0)}$$

$$= \delta_{q0} \epsilon^2 (\epsilon^2 + 2)$$

$$+ (1 - \delta_{q0}) \epsilon^2 \left(2 \sum_{\nu} \left| \bar{\eta}_q^{(k_1 + k_2, \nu)} \right|^4 \right.$$

$$\left. + \frac{\epsilon^2}{2} \sum_{\nu} \left| \bar{\eta}_{2q}^{(2k_2, \nu)} \right|^2 \left| \bar{\eta}_0^{(2k_2, \nu)} \right|^2 \right)$$

$$\times \frac{1}{\sum_{\nu} \left| \bar{\eta}_0^{(2k_1, \nu)} \right|^4},$$

where $q \equiv (k_1 - k_2)/2$. Explicitly performing the sums

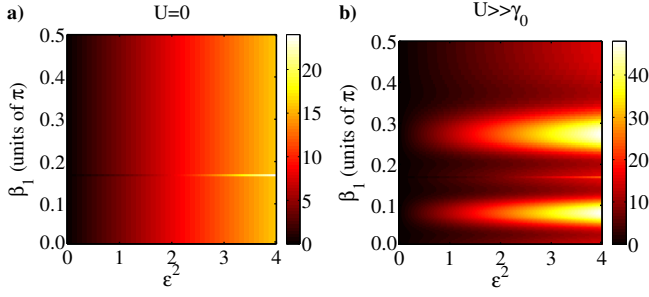


FIG. 10. (color online). Relative difference of the normalized far-field intensity for zero and non-zero second driving field, i.e., $\delta\tilde{G}_{\text{NL}}^{(1)}(\beta_1, \beta_2, \epsilon)$ according to Eq. (103) (in the limit of many atoms). We have chosen $\lambda_{\text{atom}}/a = 0.5$ and $\beta_2 = \arcsin(\lambda_{\text{at}}/a)$. The signatures for the two cases of non-interacting ($U = 0$, a)) and strongly interacting atoms ($U \gg \gamma_0$, b)) are clearly different. See the main text for the identification and discussion of the individual features.

(see App. G), we arrive at

$$\begin{aligned} \delta\tilde{G}_{\text{NL}}^{(1)}(\beta_1, \beta_2, \epsilon)/\epsilon^2 &= \delta_{q0} (\epsilon^2 + 2) \\ &+ (1 - \delta_{q0}) \begin{cases} 4 & \text{for } U = 0 \\ \frac{\frac{4}{3} \cos^4(qa) + 4 \sin^4(qa) + \frac{32}{M^2} \cos^4(qa)}{\frac{1}{3} + \frac{16}{M^2}} & \text{for } U \gg \gamma_0 \end{cases} \\ &\stackrel{M \gg 1}{\simeq} \delta_{q0} (\epsilon^2 + 2) \\ &+ 4(1 - \delta_{q0}) \begin{cases} 1 & \text{for } U = 0 \\ \cos^4(qa) + 3 \sin^4(qa) & \text{for } U \gg \gamma_0 \end{cases} \\ &+ (1 - \delta_{q0}) \begin{cases} 0 & \text{for } U = 0 \\ \frac{96}{M^2} \cos^4(qa) & \text{for } U \gg \gamma_0 \end{cases}. \end{aligned} \quad (103)$$

Also here, signatures emerging from a bound state (last line in Eq. (103), see App. G for details) appear as a small correction to the $M \gg 1$ -limit. In Fig. 10, we plot the quantity (103) (for $\lambda_{\text{atom}}/a = 0.5$) in the limit of many atoms (such that the last line in Eq. (103) vanishes). For simplicity, we choose the second driving field to impinge under an angle such that it excites a zero wavenumber mode, e.g., $\beta_2 = \arcsin(\lambda_{\text{at}}/a)$ (which translates into $k_2 = 0$ and, therefore, $q = k_1/2$). The individual peaks in Fig. 10 as a function of the angle β_1 can be identified as follows. According to Eq. (49), we have

$$\beta_1 = \arcsin \left[\frac{\lambda_{\text{at}}}{a} \left(\frac{qa}{\pi} + n \right) \right] \quad (n = 0, \pm 1, \dots). \quad (104)$$

The level scheme for the reduced Hilbert space of the driven states (as shown in Fig. 9) effectively reduces to the situation of a single pump (cf. Fig. 8) when $k_1 = k_2$, which is realized here for $q = 0$. From the properties of the momentum distributions (35)–(37), we know that for both $U = 0$ and $U \gg 0$ only the background fluorescence contributes at the argument $q = 0$. Employing Eq. (104) for $\lambda_{\text{at}}/a = 0.5$, the first Bragg order ($n = 1$)

of this background fluorescence is the peak visible at $\beta_1/\pi = 1/6 \simeq 0.17$ in both Figs. Fig. 10a) and b). In contrast to this, the decay channel for the direct fluorescence, which only occurs for $U \gg \gamma_0$ (Fig. 10b)), has its maximum contribution for $q = \pi/2a$. The corresponding $n = 0$ -order for $q = \pi/2a$ yields the peak at $\beta_1/\pi \simeq 0.08$ Fig. 10b), whereas the first Bragg order ($n = 1$) results in $\beta_1/\pi \simeq 0.27$.

On the whole, the additional degrees of freedom in the context of a two-pump setup (i.e., two angles and a relative strength between the two pumps) open up a way to reveal the scattering states' properties of direct and background fluorescence from a suitably normalized far-field intensity. This possibility is absent if one had only a single pump (as discussed in Sec. IV B). However, in contrast to the two-body bound states, the band of scattering states is quasi-degenerate (see Fig. 2) such that scattering states with different relative wavenumbers overlap spectrally. As a result, it is not possible to extract the full momentum distribution of an individual scattering state. Instead, the far-field signature is a superposition from scattering states with different relative wavenumbers (see the sum over ν in Eq. (102)). Signatures from a bound state are suppressed as $1/M^2$ in the limit of many atoms.

2. Emission Spectrum around $\omega = \omega_0 + U$

Analogous to Sec. IV B 2, the steady-state emission spectrum for the two-pump scheme recorded at the position \mathbf{r}_1 around the frequency $\omega = \omega_0 + U$ reads (see App. D for details)

$$\frac{S(\mathbf{r}_1, \omega = \omega_0 + U)\gamma_0}{2\xi^2 |\mathbf{w}(\mathbf{r}_1)|^2 M} = \frac{16\Xi^2}{3M^2} [(1 + \epsilon^4 \delta_{q0}) + 2\epsilon^2 \cos^4(qa)]. \quad (105)$$

Along the same lines as in the previous section, we define the relative difference for zero and non-zero second driving field as

$$\begin{aligned} \delta S(\beta_1, \beta_2, \epsilon, \omega = \omega_0 + U) &\equiv \\ \frac{S(\mathbf{r}_1, \omega = \omega_0 + U)|_{\epsilon \neq 0} - S(\mathbf{r}_1, \omega = \omega_0 + U)|_{\epsilon = 0}}{S(\mathbf{r}_1, \omega = \omega_0 + U)|_{\epsilon = 0}} \\ &= \epsilon^2 (\epsilon^2 \delta_{q0} + 2 \cos^4(qa)). \end{aligned} \quad (106)$$

This expression represents an approach which is complementary to the signature (85) we obtained in the context of spontaneous emission or the emission spectrum (96) for a single-pump setup. Unlike in Eqs. (85) and (96) where we relied on the collection of spontaneously emitted light, the bound state signature here is a consequence of collected photons which correspond to transitions directly driven by the external pumps (see the introduction of Sec. IV C for the choice of the detector positions).

In Fig. 11, we visualize the bound state signature according to Eq. (106). Similarly to Fig. 10, the positions

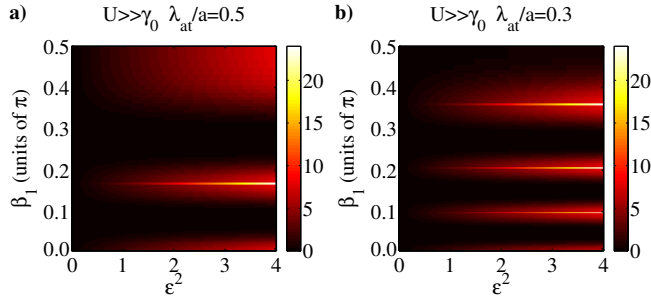


FIG. 11. (color online). Spectral signature $\delta S(\beta_1, \beta_2, \epsilon, \omega = \omega_0 + U)$ of a bound state as a function of the detection angle according to Eq. (106). As the bound states' momentum distribution has a maximum at the argument $q = 0$ (see Sec. II C 2), we observe peaks around (see also the discussion in Sec. IV C 1) $\beta_1/\pi \simeq 0, 0.17, 0.5$ (for $\lambda_{\text{at}}/a = 0.5$, a)). For $\lambda_{\text{at}}/a = 0.3$ (b)), we have $\beta_1/\pi \simeq 0, 0.10, 0.20, 0.36$.

of the peaks can be determined according to Eq. (104). The bound state's momentum distribution (37) has a maximum at the argument $q = 0$. Employing Eq. (104) for $\lambda_{\text{at}}/a = 0.5$, this leads to the peaks around $\beta_1/\pi = 0$ ($n = 0$), $\beta_1/\pi \simeq 0.17$ ($n = 1$), and $\beta_1/\pi \simeq 0.5$ ($n = 2$), which can be seen in Fig. 11a). Likewise, for a smaller wavelength $\lambda_{\text{at}}/a = 0.3$ more Bragg orders become visible at $\beta_1/\pi = 0$ ($n = 0$), $\beta_1/\pi \simeq 0.10$ ($n = 1$), $\beta_1/\pi \simeq 0.20$ ($n = 2$), and $\beta_1/\pi \simeq 0.36$ ($n = 3$) in Fig. 11b).

In the next section, we conclude our investigations on the two-pump setup with some thoughts on the measurement of consecutive photon counts. Within this framework, we analyze, as a complement to the previous studies, what can be learned from the intensity correlations with respect to the detection angle.

3. Intensity Correlations

We envision a coincidence detection scheme, where two detectors are positioned out-of-plane (y - z plane) at \mathbf{r}_1 and \mathbf{r}_2 , respectively. The two detectors have the same distance to the origin (i.e., $|\mathbf{r}_1| = |\mathbf{r}_2|$) and we aim at events with zero time delay ($\tau = 0$). Note that the detection angles are chosen such that they are equal to the excitation angles (see introduction of Sec. IV C).

According to Eq. (56), the intensity correlation function is

$$\begin{aligned} \frac{G^{(2)}(\mathbf{r}_1, \mathbf{r}_2)}{\xi^4 |\mathbf{w}(\mathbf{r}_1)|^2 |\mathbf{w}(\mathbf{r}_2)|^2 M^2} &= \sum_{\nu} \left| \bar{\eta}_{\frac{1}{2}(k_1 - k_2)}^{(k_1 + k_2, \nu)} \right|^2 N_{k_1 + k_2, \nu; k_1 + k_2, \nu} \\ &= \Xi^2 \left(\delta_{k_1 k_2} \frac{(1 + \epsilon^2)^2}{2} + (1 - \delta_{k_1 k_2}) \epsilon^2 \right) \sum_{\nu} \left| \bar{\eta}_{\frac{1}{2}(k_1 - k_2)}^{(k_1 + k_2, \nu)} \right|^4 \end{aligned}$$

To arrive at the normalized correlation function, we use

$$\frac{G^{(1)}(\mathbf{r}_1)}{\xi^2 |\mathbf{w}(\mathbf{r}_1)|^2 M} = \Xi (1 + \delta_{k_1 k_2} \epsilon^2) + \mathcal{O}(\Xi^2), \quad (107)$$

$$\frac{G^{(1)}(\mathbf{r}_2)}{\xi^2 |\mathbf{w}(\mathbf{r}_2)|^2 M} = \Xi (\epsilon^2 + \delta_{k_1 k_2}) + \mathcal{O}(\Xi^2), \quad (108)$$

leading to

$$\begin{aligned} \frac{G^{(1)}(\mathbf{r}_1)}{\xi^2 |\mathbf{w}(\mathbf{r}_1)|^2 M} \cdot \frac{G^{(1)}(\mathbf{r}_2)}{\xi^2 |\mathbf{w}(\mathbf{r}_2)|^2 M} &= \\ \Xi^2 \left[\delta_{k_1 k_2} (1 + \epsilon^2)^2 + (1 - \delta_{k_1 k_2}) \epsilon^2 \right] &+ \mathcal{O}(\Xi^3). \end{aligned} \quad (109)$$

According to Eq. (57), the normalized correlation function reads (taking into account orders up to $\mathcal{O}(\Xi^2)$ for both the nominator and the denominator)

$$g^{(2)}(\beta_1, \beta_2) = \left(1 - \frac{1}{2} \delta_{k_1 k_2} \right) \sum_{\nu} \left| \bar{\eta}_{\frac{1}{2}(k_1 - k_2)}^{(k_1 + k_2, \nu)} \right|^4. \quad (110)$$

Performing the sum over ν (see App. G for details), we finally arrive at

$$\begin{aligned} g^{(2)}(\beta_1, \beta_2) &= \frac{1}{6} \delta_{q0} \\ &+ \frac{2}{3} (1 - \delta_{q0}) \begin{cases} 1 & \text{for } U = 0 \\ \cos^4(qa) + 3 \sin^4(qa) & \text{for } U \gg \gamma_0 \end{cases} \\ &+ \begin{cases} 0 & \text{for } U = 0 \\ \frac{16}{M^2} (1 - \frac{1}{2} \delta_{q0}) \cos^4(qa) & \text{for } U \gg \gamma_0 \end{cases}, \end{aligned} \quad (111)$$

where again $q \equiv (k_1 - k_2)/2$ (which depends on β_1 and β_2). This correlation function measures two photon counts with zero time delay at the detection angles β_1 and β_2 . Note that our two-pump setup is such that excitation and detection angles coincide. Hence, varying β_1 and β_2 represents a simultaneous change of both the detection and excitation angles.

As before, the contribution from a bound state (last line in (111)) appears as a correction to the $M \gg 1$ -limit and is suppressed as $1/M^2$. Still, this correlation function provides some very characteristic features for the two cases of non-interacting atoms ($U = 0$) and strong atom-atom interactions ($U \gg \gamma_0$). For $U = 0$, the intensity correlation is essentially flat. This can again be seen as a consequence of the momentum distribution being featureless for $U = 0$ (cf. Fig. 3b)). The correlation function only jumps between the values $1/6$ and $2/3$ if the atomic system's level scheme undergoes the sudden change from an effective single-pump setup ($q = 0$, degenerate pump fields) to a two-pump setup ($q \neq 0$). In contrast to this, for $U \gg \gamma_0$, we observe a continuous angle-dependence because the underlying relevant momentum distributions also exhibit contributions from the decay channel of direct fluorescence (cf. Fig. 3c)). Also here, we can see jumps to the value of $1/6$ that occurs at angles where the pump fields are degenerate ($q = 0$). We depict these findings in Fig. 12 for $\lambda_{\text{at}}/a = 0.5$ and $\lambda_{\text{at}}/a = 0.3$. The features of Fig. 12a) are visible at the same angles as in Fig. 10, which can be calculated from Eq. (104). When compared to Fig. 12a), Fig. 12b) features more peaks because the smaller wavelength of $\lambda_{\text{at}}/a = 0.3$ allows for the observation of more Bragg orders.

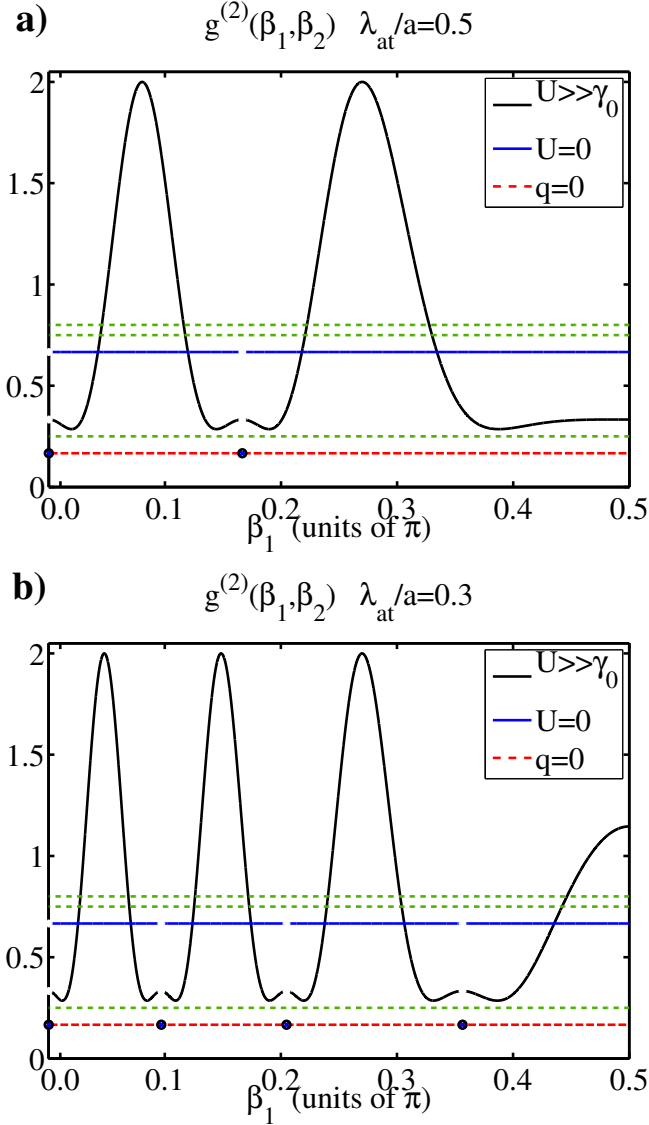


FIG. 12. (color online). Normalized photon-photon correlation function $g^{(2)}(\beta_1, \beta_2 = \arcsin(\lambda_{\text{at}}/a))$ according to Eq. (111) in the limit of many atoms (such that the last line in Eq. (111) vanishes). For $U = 0$ (blue line), the correlation function exhibits a constant value of $2/3$, except for angles where $q = 0$ is realized (red crosses). For $U \gg \gamma_0$ (black line), the $g^{(2)}$ -function varies smoothly with respect to the angle β_1 , but is also interrupted when $q = 0$ (red crosses). At $q = 0$, the correlation function always has a value of $1/6$ (denoted by the red dashed line) for both $U = 0$ and $U \gg \gamma_0$. The green dashed lines indicate reference values from Refs. [57–61], referring to a two-atom system (see text for discussion).

The sharp jumps in Fig. 12 due to the “collapse” from a two-pump scheme to the Hilbert space accessible by a single pump refer to the case of infinitely sharp excitation and detection angles. In practice, finite apertures will eventually lead to a smoothening of the curves (imagine averaging over a small angular window).

We conclude the discussion of the zero time delay in-

tensity correlation function by referring to results which have been obtained for the case of two atoms. Generally, as a consequence of spatial interference effects as pointed out in Refs. [57, 58], the values of the $g^{(2)}$ -function depend on the direction of observation and on the distance between the two atoms. In the case of a weak driving field, the zero-time delay intensity correlation $g^{(2)}(0)$ for the same detection geometry as described in this section (the two atoms are aligned along the z -axis) has the value $g^{(2)}(0) = 1/4$ [57–59] (see the corresponding green dashed line in Fig. 12). Interestingly, $g^{(2)}(0) = 3/4$ would be observed in the limit of a strong driving field in the case of zero detuning [60]. This value would drop down to $g^{(2)}(0) = 1/4$ if the driving field is tuned far off-resonant [60]. In the context of spontaneous emission from two initially excited and independent (i.e., uncoupled) atoms, the zero-time correlation function yields a value of $g^{(2)}(0) = 4/5$ [61]. Likewise, going beyond two atoms, the spontaneous emission from M independent atoms (that are initially all in the excited state) results in $g^{(2)}(0) = 1 - 1/M$ [61], which is exactly the same expression one would also obtain for an M -photon Fock state of a single-mode radiation field [55].

V. CONCLUSION

In conclusion, we have analyzed the characteristic, angle-dependent far-field signatures emerging from the excitation of collective few-excitation atomic states in the context of a one-dimensional lattice of (interacting) two-level atoms. Compared to state-of-the-art experimental techniques that rely on single-atom addressability and/or manipulation, the schemes presented in this paper represents an alternative approach for studying collective phenomena in a quantum-optical context.

In particular, we started in Sec. II with the static properties of the underlying model system. This included an in-depth discussion of the dissipative eigenstates in the submanifold of one and two atomic excitations. We put special emphasis on the distinction between the two classes of possible two-excitation states, i.e., two-excitation scattering states (which can be thought of as two colliding spin waves) and two-body bound states whose relative wavefunction is spatially localized (with respect to the relative coordinate of the two excitations). We then showed that characteristic key quantities such as the collective dipole moments, branching ratios, and, most importantly, the momentum distribution of the collective states’ relative wavefunctions are intimately linked to each other. Moreover, an expansion of the operator for the electric far field in terms of the collective atomic eigenbasis allowed us to construct operators for the emitted intensity, the emission spectrum, and an intensity correlation function.

In Sec. III, we continued with the angle-dependent far-field pattern emerging from the spontaneous emission of the system’s eigenstates. We especially discussed the

characteristic differences of the light emitted by two-body scattering states and bound states, arguing that the emission patterns can serve as a distinct fingerprint for identifying and proofing the existence of certain eigenstates on the lattice. In the course of the discussion, we also contrasted the differences between the two cases of non-interacting atoms and strong atom–atom interactions. Further, we pointed out how one could in principle extract the relative wave function’s complete momentum distribution from the far-field pattern. This is particularly appealing for the case of strong interactions, where a tightly confined two-body bound state exists.

However, since the preparation of a pure eigenstate for studying its spontaneous emission may, admittedly, pose severe challenges from a practical point of view, we turned to the investigation of the atomic system’s response to a weak and incoherent driving field in Sec. IV. Starting from an external pump field with a single spatial Fourier component, we explained the relevant excitation and relaxation mechanisms and identified the corresponding reduced level scheme. Within this framework of a single-pump setup, we were able to extract signatures for the existence of a two-body bound state from the steady-state intensity and emission spectrum in the far field.

Still, this scheme failed to reveal detailed information on the characteristics of the involved scattering states. As another approach to inferring information on the collective atomic eigenstates from the far field, we therefore extended the scheme to a special two-pump setup, where detectors were chosen such that they exclusively detect photons from driven transitions. With regard to the detected steady-state intensity and emission spectrum, the Hilbert space accessible to the external fields now not only results in a distinct signature for the existence of a bound state. Unlike for a single pump, we were also able to identify features that stem from the scattering states’ momentum distribution and which are related to the decay channels which we termed “background fluorescence” and “direct fluorescence”. However, due to the spectral overlap of scattering states with different relative wavenumbers it is not possible to extract the momentum distribution of a single scattering state and we were instead left with far-field observables resulting from the superposition of different scattering states. Moreover, we also contrasted the results for the two cases of non-interacting atoms and strong atom–atom interactions, which exhibit very different far-field patterns. In addition to that, we showed that in the framework of such a two-pump setup, an angle-dependent intensity correlation function represents another tool for analyzing the scattering states’ properties for both interacting and non-interacting atoms.

Future studies might include the dynamics induced by one or more coherent driving fields, requiring a description beyond the rate equations utilized in this work. In the context of coherent fields, an analysis of how interference effects modify the far-field emission patterns dis-

cussed in this paper would be highly interesting. This would also address whether these signatures may reveal additional or complimentary information on the properties of the collective few-excitation wavefunction. Besides that, going from weak driving fields to higher pump powers would in principle open up a way to probe the more complicated Hilbert space beyond two-excitations, which is still largely unexplored in detail. Finally, our analysis provides a promising approach to the theoretical modeling and understanding of recent experiments in nuclear quantum optics on a microscopic level.

Appendix A: Integrating out the Photonic Degrees of Freedom

The Heisenberg equations of motion for Hamiltonian (1) read

$$i\partial_t a_k = \epsilon_k a_k + \sum_n g_{nk}^* \sigma_n^-, \quad (\text{A1})$$

$$i\partial_t \sigma_n^- = -\omega_n \sigma_n^- - \sum_k g_{nk} \sigma_n^z a_k + \frac{1}{2} \sum_m V_{|n-m|} \sigma_m^+ \sigma_m^- \sigma_n^-. \quad (\text{A2})$$

Transforming to a rotating frame (i.e., $a_k \rightarrow a_k e^{-i\epsilon_k t}$, $\sigma_i^- \rightarrow \sigma_i^- e^{-i\omega_i t}$), formally integrating Eq. (A1), tracing out the photonic degrees of freedom (we assume the reservoir to be initially in the vacuum state), and inserting the result back into Eq. (A2), we arrive at the integro-differential equation for the atomic operators:

$$\partial_t \sigma_n^-(t) = \int_0^t dt' \sum_m K_{nm}(t, t') \sigma_n^z(t) \sigma_m^-(t') - \frac{i}{2} \sum_m V_{|n-m|} \sigma_m^+(t) \sigma_m^-(t) \sigma_n^-(t). \quad (\text{A3})$$

Here, $K_{nm}(t, t')$ denotes a memory kernel, which we assume to describe atom–photon coupling to a featureless continuum of modes. In other words, we apply a Markov approximation, which reduces the memory kernel to a set of complex rates, i.e.,

$$K_{nm}(t - t') = \frac{\Gamma_{|n-m|}}{2} \delta(t - t') \quad (\text{A4})$$

(the details of the rates depend on the reservoir, see Eqs. (4)–(8)), turning Eq. (A3) into

$$\partial_t \sigma_n^- = \frac{1}{2} \sum_m \Gamma_{|n-m|} \sigma_n^z \sigma_m^- - \frac{i}{2} \sum_m V_{|n-m|} \sigma_m^+ \sigma_m^- \sigma_n^-. \quad (\text{A5})$$

Hamiltonian (2) is the effective non-Hermitian Hamiltonian corresponding to the equations of motion (A5).

Appendix B: Eigenequations

1. Single-Excitation Eigenstates

The eigenproblem with respect to Hamiltonian (2) for a single-excitation state

$$|\varphi\rangle = \sum_n \varphi_n \sigma_n^+ |0\rangle \quad (\text{B1})$$

yields the difference equation

$$0 = -\frac{i}{2} \sum_m \Gamma_{|n-m|} \varphi_m - E \varphi_n. \quad (\text{B2})$$

Note that the atom-atom interaction terms are absent in the single-excitation submanifold.

2. Two-Excitation Eigenstates

The eigenproblem with respect to Hamiltonian (2) for a two-excitation state

$$|\Phi\rangle = \sum_{n_1 n_2} \Phi_{n_1 n_2} \sigma_{n_1}^+ \sigma_{n_2}^+ |0\rangle, \quad (\text{B3})$$

which we rewrite as a product of the center-of-mass motion (described by a plane wave with a center-of-mass wavenumber K) and a relative wavefunction $\Psi_{|n_1-n_2|}^{(K\nu)}$, i. e.,

$$|K\nu\rangle = \frac{1}{2\sqrt{M}} \sum_{n_1 n_2} e^{i\frac{Ka}{2}(n_1+n_2)} \cdot \Psi_{|n_1-n_2|}^{(K\nu)} \sigma_{n_1}^+ \sigma_{n_2}^+ |0\rangle, \quad (\text{B4})$$

reduces to an effective single-particle problem on a half-infinite lattice ($x > 0$, $\Psi_0^{(K\nu)} = 0$):

$$0 = -i \sum_{j \neq x} \Gamma_j \cos\left(\frac{Kaj}{2}\right) \left(\Psi_{|x-j|}^{(K\nu)} + \Psi_{|x+j|}^{(K\nu)}\right) + (V_x - E - i\Gamma_0) \Psi_x^{(K\nu)}. \quad (\text{B5})$$

Here, $K/2$ is from the first Brillouin zone and ν is a quantum number still to be determined (see main text). Note that for each center-of-mass wavenumber K the effective particle “sees” a different lattice (different hopping terms). The two-body atom-atom interaction terms now play the role of a potential for the effective particle. For the tight-binding Hamiltonian (3), the difference equation simplifies to ($x > 0$)

$$0 = -i\Gamma_1 \cos\left(\frac{Ka}{2}\right) \left(\Psi_{x-1}^{(K\nu)} + \Psi_{x+1}^{(K\nu)}\right) + (U\delta_{x,1} - E - i\Gamma_0) \Psi_x^{(K\nu)}. \quad (\text{B6})$$

Appendix C: Expansion of the Atomic Operator σ_n^- in the Eigenbasis

We transform the operator σ_n^- to the basis of the system's single- and two-excitation eigenstates by virtue of the expansion

$$\begin{aligned} \sigma_n^- &= \sum_k |0\rangle \underbrace{\langle 0 | \sigma_n^- | k \rangle}_{=\frac{1}{\sqrt{M}} e^{ik a n}} \langle k| \quad (\text{C1}) \\ &+ \sum_{k; K\nu} |k\rangle \underbrace{\langle k | \sigma_n^- | K\nu \rangle}_{=\langle k | \sum_{x_1 x_2} \Phi_{x_1 x_2} \sigma_n^- \sigma_{x_1}^+ \sigma_{x_2}^+ | 0 \rangle} \langle K\nu| \\ &= \frac{1}{\sqrt{M}} \sum_k e^{ik a n} \hat{S}_{0;k} \\ &+ 2 \sum_{k; K\nu} \sum_{m=-N/2}^{N/2} \underbrace{\Phi_{nm}}_{\frac{1}{2\sqrt{M}} e^{i\frac{Ka}{2}(n+m)} \Psi_{n-m}^{(K\nu)}} \underbrace{\langle k | \sigma_m^+ | 0 \rangle}_{\frac{1}{\sqrt{M}} e^{-ik a m}} \hat{S}_{k;K\nu} \\ &= \frac{1}{\sqrt{M}} \sum_k e^{ik a n} \hat{S}_{0;k} \\ &+ \frac{1}{2\sqrt{M}} \sum_k \sum_{K\nu} e^{i(K-k)an} \eta_{\frac{K}{2}-k;n}^{(K\nu)} \hat{S}_{k;K\nu}, \end{aligned} \quad (\text{C2})$$

where $\hat{S}_{0;k} = |0\rangle \langle k|$ and $\hat{S}_{k;K\nu} = |k\rangle \langle K\nu|$. The quantum number ν runs over all scattering states ($\nu = p$) and a possible bound state ($\nu = \text{BS}$).

The quantity

$$\eta_{q;n}^{(K\nu)} = \frac{2}{\sqrt{M}} \sum_{z=-N/2-n}^{N/2-n} e^{iqaz} \Psi_z^{(K\nu)} \quad (\text{C3})$$

may be interpreted as the windowed Fourier lattice transform of the relative wavefunction (with respect to the relative coordinate). According to Sec. IID, the electric field operator in the eigenbasis involves a sum over all atom positions, which is of the form

$$\begin{aligned} \hat{\mathbf{E}}^{(-)}(\mathbf{r}, t) &= \xi \mathbf{w}_0(\mathbf{r}) \sum_{nk} \left(\dots \right. \\ &+ \sum_{K\nu} \frac{1}{2\sqrt{M}} e^{-i\left(K-k+\frac{\Delta K\nu}{c} \sin \beta_{\text{det}}\right)an} \left(\eta_{\frac{K}{2}-k;n}^{(K\nu)} \right)^* \\ &\quad \times \hat{S}_{K\nu;k} \left(t - \frac{r}{c} \right) \Bigg). \end{aligned}$$

Performing the sum over n yields

$$\begin{aligned} \hat{\mathbf{E}}^{(-)}(\mathbf{r}, t) &= \xi \mathbf{w}(\mathbf{r}) \sum_k \left(\dots \right. \\ &+ \sqrt{M} \sum_{K\nu} \left(\bar{\eta}_{\frac{K}{2}-k}^{(K\nu)} \right)^* \delta_{k\bar{k}} \hat{S}_{K\nu;k} \left(t - \frac{r}{c} \right) \Bigg), \end{aligned}$$

where we now have the “reduced” quantity $\bar{\eta}_{\frac{K}{2}-k}^{(K\nu)}$, which is defined via

$$\frac{1}{2M} \sum_{n=-N/2}^{N/2} e^{i\kappa a n} \eta_{q;n}^{(K,\nu)} = \bar{\eta}_q^{(K,\nu)} \delta_{[\kappa]_{\frac{2\pi}{a}}, 0}. \quad (C4)$$

We will discuss $\bar{\eta}_{q;n}^{(K\nu)}$ and $\bar{\eta}_q^{(K\nu)}$ in more detail in App. E.

Appendix D: Expectation Value of the Field-Field Auto Correlation

In order to arrive at an expression for $G^{(1)}(\mathbf{r}, t, t + \tau) = \langle \hat{G}^{(1)}(\mathbf{r}, t, t + \tau) \rangle$, where

$$\begin{aligned} \hat{G}^{(1)}(\mathbf{r}, t, t + \tau) &\equiv \hat{\mathbf{E}}^{(-)}(\mathbf{r}, t) \hat{\mathbf{E}}^{(+)}(\mathbf{r}, t + \tau) \\ &= \xi^2 |\mathbf{w}(\mathbf{r})|^2 M \\ &\quad \times \left(\hat{S}_{\bar{k};0}(t_{\text{ret}}) \hat{S}_{0;\bar{k}}(t_{\text{ret}} + \tau) \right. \\ &\quad + \sum_{K\nu} \bar{\eta}_{\frac{K}{2}-\bar{k}}^{(K\nu)} \hat{S}_{\bar{k};0}(t_{\text{ret}}) \hat{S}_{K-\bar{k};K\nu}(t_{\text{ret}} + \tau) \\ &\quad + \sum_{K\nu} \left(\bar{\eta}_{\frac{K}{2}-\bar{k}}^{(K\nu)} \right)^* \hat{S}_{K\nu;K-\bar{k}}(t_{\text{ret}}) \hat{S}_{0;\bar{k}}(t_{\text{ret}} + \tau) \\ &\quad + \sum_{K\nu} \sum_{K'\nu'} \left(\bar{\eta}_{\frac{K}{2}-\bar{k}}^{(K\nu)} \right)^* \bar{\eta}_{\frac{K'}{2}-\bar{k}}^{(K'\nu')} \\ &\quad \times \hat{S}_{K\nu;K-\bar{k}}(t_{\text{ret}}) \hat{S}_{K'-\bar{k};K'\nu'}(t_{\text{ret}} + \tau) \Big), \end{aligned} \quad (D1)$$

we ultimately need to calculate (cross-)correlations such as $\langle \hat{S}_{k;0}(t) \hat{S}_{0;k'}(t + \tau) \rangle$, $\langle \hat{S}_{k;0}(t) \hat{S}_{k';K\nu}(t + \tau) \rangle$, $\langle \hat{S}_{K\nu;k}(t) \hat{S}_{0;k'}(t + \tau) \rangle$, and $\langle \hat{S}_{K\nu;k}(t) \hat{S}_{k';K'\nu'}(t + \tau) \rangle$. Generally, this can be achieved by exploiting the quantum regression theorem [53], which we will use in the form (in the following, we have $t \rightarrow \infty$, denoting a steady state)

$$\begin{aligned} \langle \hat{A}(t) \hat{B}(t + \tau) \rangle_{t \rightarrow \infty} &= \sum_j \mathcal{G}_j(\tau) \langle \hat{A} \hat{B}_j \rangle_{t \rightarrow \infty}, \quad (D2) \\ \langle \hat{B}(\tau) \rangle &= \sum_j \mathcal{G}_j(\tau) \langle \hat{B}_j(0) \rangle. \end{aligned}$$

Explicitly, we have

$$\begin{aligned} \langle \hat{S}_{k;0}(t) \hat{S}_{0;k'}(t + \tau) \rangle &= \mathcal{G}_{0;k'}(\tau) \langle \hat{S}_{k;0} \hat{S}_{0;k'} \rangle \\ &= \mathcal{G}_{0;k'}(\tau) \varrho_{k';k}, \end{aligned} \quad (D3)$$

$$\begin{aligned} \langle \hat{S}_{0;k}(\tau) \rangle &= \mathcal{G}_{0;k}(\tau) \langle \hat{S}_{0;k}(0) \rangle \\ &= \mathcal{G}_{0;k}(\tau) \varrho_{k;0}(0), \end{aligned}$$

$$\begin{aligned} \langle \hat{S}_{k;0}(t) \hat{S}_{k';K\nu}(t + \tau) \rangle &= \mathcal{G}_{k';K\nu}(\tau) \langle \hat{S}_{k;0} \hat{S}_{k';K\nu} \rangle \\ &= 0, \end{aligned} \quad (D4)$$

$$\begin{aligned} \langle \hat{S}_{K\nu;k}(t) \hat{S}_{0;k'}(t + \tau) \rangle &= \mathcal{G}_{0;k'}(\tau) \langle \hat{S}_{K\nu;k} \hat{S}_{0;k'} \rangle \\ &= 0, \end{aligned} \quad (D5)$$

$$\langle \hat{S}_{K\nu;k}(t) \hat{S}_{k';K'\nu'}(t + \tau) \rangle = \mathcal{G}_{k';K'\nu'}(\tau) \langle \hat{S}_{K\nu;k} \hat{S}_{k';K'\nu'} \rangle \quad (D6)$$

$$\begin{aligned} &= \mathcal{G}_{k';K'\nu'}(\tau) \delta_{kk'} \varrho_{K'\nu';K\nu}, \\ \langle \hat{S}_{k;K\nu}(\tau) \rangle &= \mathcal{G}_{k;K\nu}(\tau) \langle \hat{S}_{k;K\nu}(0) \rangle \\ &= \mathcal{G}_{k;K\nu}(\tau) \varrho_{K\nu;k}(0). \end{aligned} \quad (D7)$$

We can extract the propagators from Eqs. (F7)–(F11), yielding

$$\mathcal{G}_{0;k}(\tau) = e^{-i\Delta_0^k \tau} e^{-\frac{1}{2}(\tilde{\Gamma}_k + \sum_n |\mathcal{P}_n|^2) \tau}, \quad (D8)$$

$$\mathcal{G}_{k;K\nu}(\tau) = e^{-i\Delta_k^{K\nu} \tau} e^{-\frac{1}{2}(\Gamma_{\text{tot}}^{K\nu} + \tilde{\Gamma}_k) \tau}, \quad (D9)$$

and therefore

$$\begin{aligned} \langle \hat{S}_{k;0}(t) \hat{S}_{0;k'}(t + \tau) \rangle &= \\ e^{-i\Delta_0^k \tau} e^{-\frac{1}{2}(\tilde{\Gamma}_k + \sum_n |\mathcal{P}_n|^2) \tau} \varrho_{k';k}, \end{aligned} \quad (D10)$$

$$\begin{aligned} \langle \hat{S}_{K\nu;k}(t) \hat{S}_{k';K'\nu'}(t + \tau) \rangle &= \\ e^{-i\Delta_k^{K\nu} \tau} e^{-\frac{1}{2}(\Gamma_{\text{tot}}^{K\nu} + \tilde{\Gamma}_k) \tau} \delta_{kk'} \varrho_{K'\nu';K\nu}. \end{aligned} \quad (D11)$$

The simplified expressions (for $\omega_0 \gg U \gg \gamma_0 \gg |\mathcal{P}_n|^2$) for the propagators are

$$\mathcal{G}_{0;k}(\tau) \simeq e^{-i\omega_0 \tau} e^{-\frac{1}{2}\gamma_0 \tau}, \quad (D12)$$

$$\mathcal{G}_{k;K\nu}(\tau) \simeq e^{-i\omega_0 \tau} e^{-\frac{3}{2}\gamma_0 \tau}, \quad (D13)$$

$$\mathcal{G}_{k;K,\text{BS}}(\tau) \simeq e^{-i(\omega_0 + U) \tau} e^{-\frac{3}{2}\gamma_0 \tau}. \quad (D14)$$

Note that in the presence of an incoherent pump, we have $\varrho_{k';k} \propto \delta_{kk'}$ and $\varrho_{K'\nu';K\nu} \propto \delta_{K\nu;K'} \delta_{\nu\nu'}$.

Hence,

$$\begin{aligned} \frac{G^{(1)}(\mathbf{r}, t, t + \tau)}{\xi^2 |\mathbf{w}(\mathbf{r})|^2 M} &= \\ \left(\mathcal{G}_{0;\bar{k}}(\tau) N_{\bar{k}} + \sum_{K\nu} \left| \bar{\eta}_{\frac{K}{2}-\bar{k}}^{(K\nu)} \right|^2 \mathcal{G}_{K-\bar{k};K\nu}(\tau) N_{K\nu} \right). \end{aligned} \quad (D15)$$

Specifically, for the single-pump setup (see Eqs. (F30)–(F31) for the nonzero occupation numbers)

$$\begin{aligned} \frac{G^{(1)}(\mathbf{r}, t, t + \tau)}{\xi^2 |\mathbf{w}(\mathbf{r})|^2 M} &= \\ \left(\mathcal{G}_{0;\bar{k}}(\tau) N_{\bar{k}} + \sum_{\nu} \left| \bar{\eta}_{k_P-\bar{k}}^{(2k_P,\nu)} \right|^2 \mathcal{G}_{2k_P-\bar{k};2k_P,\nu}(\tau) N_{2k_P,\nu} \right), \end{aligned} \quad (D16)$$

whereas for the two-pump setup as introduced in Sec. IV C we have (see App. F 2 for the steady-state solution)

$$\begin{aligned} \frac{G^{(1)}(\mathbf{r}_1, t, t + \tau)}{\xi^2 |\mathbf{w}(\mathbf{r}_1)|^2 M} &= \\ \left(\mathcal{G}_{0;k_1}(\tau) N_{k_1} + \sum_{\nu} \left| \bar{\eta}_0^{(2k_1,\nu)} \right|^2 \mathcal{G}_{k_1;2k_1,\nu}(\tau) N_{2k_1,\nu} \right. \\ \left. + (1 - \delta_{k_1 k_2}) \sum_{\nu} \left| \bar{\eta}_{\frac{1}{2}(k_1+k_2)}^{(k_1+k_2,\nu)} \right|^2 \mathcal{G}_{k_2;k_1+k_2,\nu}(\tau) N_{k_1+k_2,\nu} \right). \end{aligned} \quad (D17)$$

The Fourier transform according to Eq. (54) then finally yields the emission spectrum.

Appendix E: Calculation of $\bar{\eta}_q^{(K\nu)}$

Let us start with a closer inspection of Eq. (C3) (remember that $\Psi_0^{(K\nu)} = 0$):

$$\begin{aligned}
\eta_{q;n}^{(K\nu)} &= \frac{2}{\sqrt{M}} \sum_{z=-N/2-n}^{N/2-n} e^{iqaz} \Psi_z^{(K\nu)} \\
&= \frac{2}{\sqrt{M}} \left(\sum_{z=-N/2-n}^0 e^{iqaz} \Psi_z + \sum_{z=0}^{N/2-n} e^{iqaz} \Psi_z^{(K\nu)} \right) \\
&= \frac{2}{\sqrt{M}} \left(\sum_{z=0}^{N/2-n} e^{iqaz} \Psi_z + \sum_{z=0}^{N/2+n} e^{-iqaz} \Psi_z^{(K\nu)} \right) \\
&= \frac{2}{\sqrt{M}} \left(\theta \left(\frac{N}{2} - n - 1 \right) \sum_{z=1}^{N/2-n} e^{iqaz} \Psi_z^{(K\nu)} \right. \\
&\quad \left. + \theta \left(n + \frac{N}{2} - 1 \right) \sum_{z=1}^{N/2+n} e^{-iqaz} \Psi_z^{(K\nu)} \right) \\
&= 2 \sum_{\zeta=\pm} \theta \left(\frac{N}{2} + \zeta n - 1 \right) \sum_{z=1}^{N/2+\zeta n} \frac{e^{-i\zeta qaz}}{\sqrt{M}} \Psi_z^{(K\nu)}.
\end{aligned} \tag{E1}$$

Here, we have used the discrete version of the Heaviside step function according to $\theta(n) = 1$ if $n \geq 0$ and $\theta(n) = 0$ if $n < 0$. From Eq. (C4), we see that the quantity $\bar{\eta}_q^{(K\nu)}$ can be determined via (setting $\kappa = 0$ in Eq. (C4))

$$\begin{aligned}
\bar{\eta}_q^{(K\nu)} &= \frac{1}{2M} \sum_{n=-N/2}^{N/2} \eta_{q;n}^{(K\nu)} \\
&= \frac{1}{M} \sum_{\zeta=\pm} \sum_{n=-N/2}^{N/2} \theta \left(\frac{N}{2} + \zeta n - 1 \right) \\
&\quad \times \sum_{z=1}^{N/2+\zeta n} \frac{e^{-i\zeta qaz}}{\sqrt{M}} \Psi_z^{(K\nu)}.
\end{aligned} \tag{E2}$$

Before we proceed with the actual calculation, we need to be cautious regarding the wavefunction's boundary conditions. Usually, the boundary conditions must not play a role for a lattice with many atoms ($M \gg 1$). However, being pedantic, the eigenstates presented in Sec. II B actually do not satisfy hard-wall boundary conditions for a finite lattice (in the calculation, it is assumed that M is still finite). At the boundary, the wavefunction should actually vanish. This is not the case here as the ansatz we employed (both for single- and two-excitation states) represents open boundary conditions, i. e., in- and outgoing waves that are suited in the context of an infinite lattice. To be precise, Equations (E1) and (E2) explicitly depend on the boundary values (for instance, the term for $n = \zeta N/2$ in Eq. (E1) requires the relative wavefunction at the relative coordinate $z = N$, which may stand for two excitations at the boundaries $x_1 = N/2$ and $x_2 = -N/2$). Furthermore, the sum over z depends

on n and represents a finite “window”. If we, however, combine the demand that “integrated” quantities such as Eq. (E2) must be independent of the boundary conditions in the limit of a large (eventually infinite) lattice, we come to the conclusion that the “window length” should not affect Eqs. (E1) and (E2). Hence, we proceed with the expressions

$$\eta_{q;n}^{(K\nu)} = 2 \sum_{\zeta=\pm} \sum_{z=1}^{N/2} \frac{e^{-i\zeta qaz}}{\sqrt{M}} \Psi_z^{(K\nu)}, \tag{E3}$$

$$\bar{\eta}_q^{(K\nu)} = \frac{1}{M} \sum_{\zeta=\pm} \sum_{n=-N/2}^{N/2} \sum_{z=1}^{N/2} \frac{e^{-i\zeta qaz}}{\sqrt{M}} \Psi_z^{(K\nu)}, \tag{E4}$$

(where we additionally ignored the θ -function for similar reasons). Performing the sum over n , we are ultimately left with

$$\bar{\eta}_q^{(K\nu)} = \sum_{\zeta=\pm} \sum_{z=1}^{N/2} \frac{e^{-i\zeta qaz}}{\sqrt{M}} \Psi_z^{(K\nu)}. \tag{E5}$$

1. Scattering States ($\bar{\eta}_q^{(Kp)}$)

For scattering states, we arrive at (the Kronecker symbols $\delta_{p,\pm q}$ should not be confused with the scattering phase shift in $\exp(i\delta_{Kp})$)

$$\begin{aligned}
\bar{\eta}_q^{(Kp)} &= \sum_{\zeta=\pm} \frac{1}{M} \sum_{z=1}^{N/2} \left(e^{i(p-\zeta q)az} + e^{i\delta_{Kp}} e^{-i(p+\zeta q)az} \right) \\
&= \sum_{\zeta=\pm} \left[\frac{1}{2} (\delta_{p,\zeta q} + e^{i\delta_{Kp}} \delta_{p,-\zeta q}) \right. \\
&\quad + \frac{1}{M} (1 - \delta_{p,\zeta q}) \left(\frac{1 - e^{i(p-\zeta q)a(\frac{N}{2}+1)}}{1 - e^{i(p-\zeta q)a}} - 1 \right) \\
&\quad \left. + \frac{1}{M} (1 - \delta_{p,-\zeta q}) \left(\frac{1 - e^{-i(p+\zeta q)a(\frac{N}{2}+1)}}{1 - e^{-i(p+\zeta q)a}} - 1 \right) e^{i\delta_{Kp}} \right] \\
&= \frac{1}{2} (1 + e^{i\delta_{Kp}}) (\delta_{pq} + \delta_{p,-q}) \\
&\quad + \frac{1}{M} (1 - \delta_{pq}) \left(\frac{1 - e^{i(p-q)a\frac{N}{2}}}{e^{-i(p-q)a} - 1} + e^{i\delta_{Kp}} \frac{1 - e^{-i(p-q)a\frac{N}{2}}}{e^{i(p-q)a} - 1} \right) \\
&\quad + \frac{1}{M} (1 - \delta_{p,-q}) \left(\frac{1 - e^{i(p+q)a\frac{N}{2}}}{e^{-i(p+q)a} - 1} + e^{i\delta_{Kp}} \frac{1 - e^{-i(p+q)a\frac{N}{2}}}{e^{i(p+q)a} - 1} \right).
\end{aligned} \tag{E6}$$

During the derivation, we have used the formula for finite geometric sums, and we also assumed $M, N \gg 1$. Note the symmetry property $\bar{\eta}_q^{(Kp)} = \bar{\eta}_{-q}^{(Kp)}$. For $q \geq 0$ and

$p > 0$, we may therefore write

$$\begin{aligned} \bar{\eta}_{q \geq 0}^{(K, p > 0)} &= \frac{1 + e^{i\delta_{Kp}}}{2} \delta_{pq} \\ &+ \frac{2e^{i\frac{\delta_{Kp}}{2}}}{M} \cdot \frac{\sin\left[\frac{1}{2}(\delta_{Kp} - (p-q)a)\right]}{\sin\left[\frac{1}{2}(p-q)a\right]} \\ &\times (1 - \delta_{pq}) \left(1 - \delta_{\left[\frac{(p-q)aN}{2\pi}\right]_2, 0}\right). \end{aligned} \quad (E7)$$

During this derivation, we have exploited the fact that the difference of the wavenumbers p and q can be written as $p - q = m \cdot 2\pi/Ma$, where m is an integer. Hence, $(p - q)Na/2 \stackrel{M \gg 1}{\approx} (p - q)Ma/2 = m\pi$ and $\exp[(p - q)N/2] = (-1)^m$ so that we only have a contribution from the “background term” if m is odd (expressed through the second Krockers- δ).

2. Bound States ($\bar{\eta}_q^{(K, BS)}$)

Proceeding along the same lines for the case of a bound state, we have the expression

$$\begin{aligned} \bar{\eta}_q^{(K, BS)} &= \sum_{\zeta=\pm} \sum_{z=1}^{N/2} \frac{e^{-i\zeta q a z}}{\sqrt{M}} \alpha_K^{z-1} \\ &= \frac{1}{\sqrt{M} \alpha_K} \sum_{\zeta=\pm} \sum_{z=1}^{N/2} (e^{-i\zeta q a} \alpha_K)^z \\ &= \frac{1}{\sqrt{M} \alpha_K} \sum_{\zeta=\pm} \left(\frac{1 - (e^{-i\zeta q a} \alpha_K)^{N/2+1}}{1 - e^{-i\zeta q a} \alpha_K} - 1 \right) \\ &= \frac{2}{\sqrt{M}} \cdot \frac{\cos(qa) - \alpha_K}{1 - 2\alpha_K \cos(qa) + \alpha_K^2} \\ &\stackrel{U \gg \gamma_0}{\approx} \frac{2 \cos(qa)}{\sqrt{M}}. \end{aligned} \quad (E8)$$

In the derivation, we have exploited the fact that $\alpha_K^{N/2}$ vanishes since $N \gg 1$. In the last line, we have additionally assumed $U \gg \gamma_0$, meaning the bound state is tightly confined with respect to the relative coordinate.

3. Sum over $|\bar{\eta}_q^{(K\nu)}|^2$

Consider the quantity

$$\begin{aligned} Z^{(K\nu)} &\equiv \sum_{qa=\frac{K}{2}-\pi}^{\frac{K}{2}+\pi} |\bar{\eta}_q^{(K\nu)}|^2 = \sum_{qa=-\pi}^{\pi} |\bar{\eta}_q^{(K\nu)}|^2 \\ &= 2 \sum_{qa=0}^{\pi} |\bar{\eta}_q^{(K\nu)}|^2 - |\bar{\eta}_0^{(K\nu)}|^2 \\ &\stackrel{M \gg 1}{\approx} 2 \sum_{qa=0}^{\pi} |\bar{\eta}_q^{(K\nu)}|^2. \end{aligned} \quad (E9)$$

For scattering states, we have

$$\begin{aligned} Z^{(Kp)} &= 2 \left(\sum_{qa=0, q \neq p}^{\pi} |\bar{\eta}_q^{(Kp)}|^2 + |\bar{\eta}_p^{(Kp)}|^2 \right) \\ &= 2 \left(\cos^2\left(\frac{\delta_{Kp}}{2}\right) \right. \\ &\quad \left. + \frac{4}{M^2} \sum_{qa=0, q \neq p}^{\pi} \frac{\cos[\delta_{Kp} + (q-p)a] - 1}{\cos[(p-q)a] - 1} \right. \\ &\quad \left. \times \left(1 - \delta_{\left[\frac{(p-q)aN}{2\pi}\right]_2, 0}\right) \right). \end{aligned} \quad (E10)$$

The lattice sum can be performed in the limit $M \gg 1$. Defining $\delta \equiv 2\pi/aM \ll 1$ and rewriting $q = p + \delta \cdot n$, we essentially have to calculate

$$\frac{\delta^2}{\pi^2} \sum_n' \frac{\cos(\delta_{Kp} + \delta n) - 1}{\cos(\delta n) - 1}, \quad (E11)$$

which can be expanded into a Taylor series in δ in which only terms of order δ^0 remain in the limit $M \gg 1$, yielding

$$\frac{2}{\pi^2} (1 - \cos \delta_{Kp}) \sum_n' \frac{1}{n^2}. \quad (E12)$$

The sum runs over those odd values of n such that all wavenumbers from $0 \rightarrow p - \delta$ as well as from $p + \delta \rightarrow \pi/a$ are covered. In the limit $M \gg 1$, n runs over all odd values from 1 to ∞ as well as from -1 to $-\infty$, resulting in

$$2 \underbrace{\sum_{n=0}^{\infty} \frac{1}{(2n+1)^2}}_{\frac{\pi^2}{8}} = \frac{\pi^2}{4}. \quad (E13)$$

This eventually leads to

$$Z^{(Kp)} = 2 \cdot \left(\cos^2\left(\frac{\delta_{Kp}}{2}\right) + \frac{1}{2} (1 - \cos \delta_{Kp}) \right) = 2. \quad (E14)$$

Similarly, the calculation for a bound states is ($U \gg \gamma_0$)

$$\begin{aligned} Z^{(K, BS)} &= \sum_{qa=-\pi}^{\pi} |\bar{\eta}_q^{(K, BS)}|^2 \\ &= \frac{4}{M} \sum_{qa=-\pi}^{\pi} \cos^2(qa) \\ &\rightarrow 4 \int_{-\frac{\pi}{a}}^{\frac{\pi}{a}} \frac{dq}{2\pi} \cos^2(qa) = 2. \end{aligned} \quad (E15)$$

Hence, we can generally write $Z^{(K\nu)} = 2$.

Appendix F: Equations of Motion with Incoherent Driving Field

We can extend Eqs. (64)–(69) to account for an external, incoherent driving field, yielding the following equations of motion for the density matrix elements:

$$\partial_t \varrho_{K\nu;K'\nu'} = \left[-i\Delta_{K'\nu'}^{K\nu} - \frac{1}{2} \left(\Gamma_{\text{tot}}^{K\nu} + \Gamma_{\text{tot}}^{K'\nu'} \right) \right] \varrho_{K\nu;K'\nu'} \quad (\text{F1})$$

$$+ \delta_{K'K} \delta_{\nu\nu'} \sum_k \sum_n \delta_{K,k+k_n} |\mathcal{P}_n|^2 \left| \bar{\eta}_{\frac{1}{2}(k_n-k)}^{(k+k_n,\nu)} \right|^2 \varrho_{k;k},$$

$$\partial_t \varrho_{k;k'} = \left[-i\Delta_{k'}^k - \frac{1}{2} (\Gamma_k + \Gamma_{k'}) \right] \varrho_{k;k'} \quad (\text{F2})$$

$$- \frac{1}{2} \sum_n \sum_{\nu'} |\mathcal{P}_n|^2 \left(\left| \bar{\eta}_{\frac{1}{2}(k_n-k)}^{(k+k_n,\nu)} \right|^2 + \left| \bar{\eta}_{\frac{1}{2}(k_n-k')}^{(k'+k_n,\nu)} \right|^2 \right) \varrho_{k;k'}$$

$$+ \delta_{k,k'} \sum_n |\mathcal{P}_n|^2 \delta_{k,k_n} \varrho_{0;0}$$

$$+ \delta_{k,k'} \sum_{K'\nu'} \Gamma_k^{K'\nu'} \varrho_{K'\nu';K'\nu'},$$

$$\partial_t \varrho_{0;0} = \sum_k \Gamma_k \varrho_{k;k} - \sum_n |\mathcal{P}_n|^2 \varrho_{0;0}, \quad (\text{F3})$$

$$\partial_t \varrho_{K\nu;k} = \left[-i\Delta_k^{K\nu} - \frac{1}{2} (\Gamma_{\text{tot}}^{K\nu} + \Gamma_k) \right] \varrho_{K\nu;k} \quad (\text{F4})$$

$$- \frac{1}{2} \sum_n \sum_{\nu'} |\mathcal{P}_n|^2 \left| \bar{\eta}_{\frac{1}{2}(k_n-k)}^{(k+k_n,\nu')} \right|^2 \varrho_{K\nu;k},$$

$$\partial_t \varrho_{K\nu;0} = \left[-i\text{Re}(E_{K\nu}^{(2)}) - \frac{1}{2} \Gamma_{\text{tot}}^{K\nu} \right] \varrho_{K\nu;0} \quad (\text{F5})$$

$$- \frac{1}{2} \sum_n |\mathcal{P}_n|^2 \varrho_{K\nu;0},$$

$$\partial_t \varrho_{k;0} = \left[-i\Delta_0^k - \frac{1}{2} \Gamma_k \right] \varrho_{k;0} \quad (\text{F6})$$

$$- \frac{1}{2} \sum_n \sum_{\nu} |\mathcal{P}_n|^2 \left| \bar{\eta}_{\frac{1}{2}(k_n-k)}^{(k+k_n,\nu)} \right|^2 \varrho_{k;0}$$

$$- \frac{1}{2} \sum_n |\mathcal{P}_n|^2 \varrho_{k;0}.$$

The coherences ($K \neq K'$, $\nu \neq \nu'$, $k \neq k'$) evolve in time according to

$$\varrho_{K\nu;K'\nu'}(t) = \varrho_{K\nu;K'\nu'}(0) e^{-i\Delta_{K'\nu'}^{K\nu} t} e^{-\frac{1}{2}(\Gamma_{\text{tot}}^{K\nu} + \Gamma_{\text{tot}}^{K'\nu'})t} \quad (\text{F7})$$

$$\varrho_{k;k'}(t) = \varrho_{k;k'}(0) e^{-i\Delta_{k'}^k t} e^{-\frac{1}{2}(\tilde{\Gamma}_k + \tilde{\Gamma}_{k'})t}, \quad (\text{F8})$$

$$\varrho_{K\nu;k}(t) = \varrho_{K\nu;k}(0) e^{-i\Delta_k^{K\nu} t} e^{-\frac{1}{2}(\Gamma_{\text{tot}}^{K\nu} + \tilde{\Gamma}_k)t}, \quad (\text{F9})$$

$$\varrho_{K\nu;0}(t) = \varrho_{K\nu;0}(0) e^{-i\text{Re}(E_{K\nu}^{(2)})t} e^{-\frac{1}{2}[\Gamma_{\text{tot}}^{K\nu} + \sum_n |\mathcal{P}_n|^2]t} \quad (\text{F10})$$

$$\varrho_{k;0}(t) = \varrho_{k;0}(0) e^{-i\Delta_0^k t} e^{-\frac{1}{2}(\tilde{\Gamma}_k + \sum_n |\mathcal{P}_n|^2)t}, \quad (\text{F11})$$

where $\tilde{\Gamma}_k \equiv \Gamma_k + \sum_n \sum_{\nu} |\mathcal{P}_n|^2 \left| \bar{\eta}_{\frac{1}{2}(k_n-k)}^{(k+k_n,\nu)} \right|^2$. For $\omega_0 \gg \gamma_0 \gg |\mathcal{P}_n|^2$ we are left with

$$\varrho_{K\nu;K'\nu'}(t) \simeq \varrho_{K\nu;K'\nu'}(0) e^{-2\gamma_0 t}, \quad (\text{F12})$$

$$\varrho_{k;k'}(t) \simeq \varrho_{k;k'}(0) e^{-\gamma_0 t}, \quad (\text{F13})$$

$$\varrho_{Kp;k}(t) \simeq \varrho_{Kp;k}(0) e^{-i\omega_0 t} e^{-\frac{3}{2}\gamma_0 t}, \quad (\text{F14})$$

$$\varrho_{K,\text{BS};k}(t) \simeq \varrho_{K,\text{BS};k}(0) e^{-i(\omega_0+U)t} e^{-\frac{3}{2}\gamma_0 t}, \quad (\text{F15})$$

$$\varrho_{Kp;0}(t) \simeq \varrho_{Kp;0}(0) e^{-2i\omega_0 t} e^{-\gamma_0 t}, \quad (\text{F16})$$

$$\varrho_{K,\text{BS};0}(t) \simeq \varrho_{K,\text{BS};0}(0) e^{-i(2\omega_0+U)t} e^{-\gamma_0 t}, \quad (\text{F17})$$

$$\varrho_{k;0}(t) \simeq \varrho_{k;0}(0) e^{-i\omega_0 t} e^{-\frac{1}{2}\gamma_0 t}. \quad (\text{F18})$$

For the diagonal elements $N_m \equiv \varrho_{m;m}$, we arrive at a set of coupled rate equations, which can be compactly written as

$$[\partial_t + \Gamma_{\text{tot}}^{K\nu}] N_{K\nu} = \sum_n |\mathcal{P}_n|^2 \left| \bar{\eta}_{\frac{K}{2}-k_n}^{(K,\nu)} \right|^2 N_{K-k_n}, \quad (\text{F19})$$

$$[\partial_t + \tilde{\Gamma}_k] N_k = \sum_n |\mathcal{P}_n|^2 \delta_{kk_n} \left(1 - \sum_k N_k - \sum_{K\nu} N_{K\nu} \right) \quad (\text{F20})$$

$$+ \sum_{K\nu} \Gamma_k^{K\nu} N_{K\nu},$$

where we have exploited the conservation of the total probability

$$N_0 + \sum_k N_k + \sum_{K\nu} N_{K\nu} = 1. \quad (\text{F21})$$

Consequently, the steady state obeys

$$N_{K\nu} = \sum_n \frac{|\mathcal{P}_n|^2}{\Gamma_{\text{tot}}^{K\nu}} \left| \bar{\eta}_{\frac{K}{2}-k_n}^{(K,\nu)} \right|^2 N_{K-k_n}, \quad (\text{F22})$$

$$N_k = \sum_n \frac{|\mathcal{P}_n|^2}{\tilde{\Gamma}_k} \delta_{kk_n} \left(1 - \sum_k N_k - \sum_{K\nu} N_{K\nu} \right) \quad (\text{F23})$$

$$+ \sum_{K\nu} \frac{\Gamma_k^{K\nu}}{\tilde{\Gamma}_k} N_{K\nu}.$$

1. Steady-State Solution: Single Pump

The steady-state solution to Eqs. (F22) and (F23) for the case of a driving field with a single Fourier component (pump rate $|\mathcal{P}|^2$, “imprinted” wavenumber k_P) can be constructed as follows. We insert Eq. (F22) into Eq. (F23) and approximate $N_0 \approx 1$ (weak pump) and arrive at

$$N_k \simeq \frac{|\mathcal{P}|^2}{\tilde{\Gamma}_k} \left(\delta_{kk_P} + \sum_{K\nu} \frac{\Gamma_k^{K\nu}}{\Gamma_{\text{tot}}^{K\nu}} \left| \bar{\eta}_{\frac{K}{2}-k_P}^{(K,\nu)} \right|^2 N_{K-k_P} \right). \quad (\text{F24})$$

Evaluating this equation for $k \neq k_P$ yields the occupation of a single excitation state $|k\rangle$ that is not directly connected to the pump field and can only be populated via spontaneous emission from a driven two-excitation state. The dominant contributions in the sum on the right-hand side of Eq. (F24) is thus from the driven states with $K - k_P = k_P$. The other states ($K - k_P \neq k_P$) are of even higher order in the pump rates and may be neglected. This idea leads us to

$$N_{k \neq k_P} \simeq \frac{|\mathcal{P}|^2}{\tilde{\Gamma}_k} \sum_{\nu} \frac{\Gamma_k^{2k_P,\nu}}{\Gamma_{\text{tot}}^{2k_P,\nu}} \left| \bar{\eta}_0^{(2k_P,\nu)} \right|^2 N_{k_P}. \quad (\text{F25})$$

Conversely, if we evaluate Eq. (F24) for $k = k_P$ we may assume

$$1 \gg \sum_{K \neq 2k_P} \sum_{\nu} \frac{\Gamma_k^{K\nu}}{\Gamma_{\text{tot}}^{K\nu}} \left| \bar{\eta}_{\frac{K}{2}-k_P}^{(K\nu)} \right|^2 N_{K-k_P} \quad (\text{F26})$$

so that

$$N_{k=k_P} \simeq \frac{|\mathcal{P}|^2}{\tilde{\Gamma}_{k_P}} \left(1 + \sum_{\nu} \frac{\Gamma_{k_P}^{2k_P,\nu}}{\Gamma_{\text{tot}}^{2k_P,\nu}} \left| \bar{\eta}_0^{(2k_P,\nu)} \right|^2 N_{k_P} \right). \quad (\text{F27})$$

Up to second order in the pump rates, we can therefore write (remember $1/(1-x) \approx 1+x$, $x \ll 1$)

$$N_{k=k_P} \simeq \frac{|\mathcal{P}|^2}{\tilde{\Gamma}_{k_P}} + \left(\frac{|\mathcal{P}|^2}{\tilde{\Gamma}_{k_P}} \right)^2 \sum_{\nu} \frac{\Gamma_{k_P}^{2k_P,\nu}}{\Gamma_{\text{tot}}^{2k_P,\nu}} \left| \bar{\eta}_0^{(2k_P,\nu)} \right|^2. \quad (\text{F28})$$

Inserted back into Eq. (F25), we arrive at

$$N_{k \neq k_P} \simeq \frac{|\mathcal{P}|^2}{\tilde{\Gamma}_k} \frac{|\mathcal{P}|^2}{\tilde{\Gamma}_{k_P}} \sum_{\nu} \frac{\Gamma_k^{2k_P,\nu}}{\Gamma_{\text{tot}}^{2k_P,\nu}} \left| \bar{\eta}_0^{(2k_P,\nu)} \right|^2 \quad (\text{F29})$$

for the undriven single-excitation states. Going back to Eq. (F22) and using the previous results, we see that the dominant terms on the right-hand side stem from $K = 2k_P$. Any other K value implies a scaling with the third power in the pump rates, which we neglect.

For $\omega_0 \gg \gamma_0$, we can then finally write

$$N_k \simeq \Xi \delta_{kk_P} + \Xi^2 \sum_{\nu} b_k^{(2k_P,\nu)} \left| \bar{\eta}_0^{(2k_P,\nu)} \right|^2 \quad (\text{F30})$$

$$= \Xi \delta_{kk_P} + \frac{\Xi^2}{2} \sum_{\nu} \left| \bar{\eta}_{k_P-k}^{(2k_P,\nu)} \right|^2 \left| \bar{\eta}_0^{(2k_P,\nu)} \right|^2,$$

$$N_{K\nu} \simeq \frac{\Xi^2}{2} \left| \bar{\eta}_0^{(2k_P,\nu)} \right|^2 \delta_{K,2k_P}, \quad (\text{F31})$$

where $\Xi \equiv |\mathcal{P}|^2/\gamma_0$.

2. Steady-State Solution: Two Pumps

Using the same reasoning as in App. F 1, the steady-state occupation numbers can be obtained for the case of an external field with two spatial Fourier components. The pump rates are, respectively, $|\mathcal{P}_1|^2 \equiv |\mathcal{P}|^2$ and $|\mathcal{P}_2|^2 \equiv \epsilon^2 |\mathcal{P}|^2$, and k_1 and k_2 denote the “imprinted” wavenumbers. We only need the solution for wavenumbers $K = 2k_1, 2k_2, k_1 + k_2$ and $k = k_1, k_2$ (see main text).

For $k_1 \neq k_2$, the solution reads (again, $\Xi \equiv |\mathcal{P}|^2/\gamma_0$)

$$N_{2k_1,\nu} \simeq \frac{\Xi^2}{2} \left| \bar{\eta}_0^{(2k_1,\nu)} \right|^2, \quad (\text{F32})$$

$$N_{2k_2,\nu} \simeq \epsilon^4 \frac{\Xi^2}{2} \left| \bar{\eta}_0^{(2k_2,\nu)} \right|^2, \quad (\text{F33})$$

$$N_{k_1+k_2,\nu} \simeq \epsilon^2 \Xi^2 \left| \bar{\eta}_{\frac{1}{2}(k_1-k_2)}^{(k_1+k_2,\nu)} \right|^2, \quad (\text{F34})$$

$$N_{k_1} \simeq \Xi + \frac{\Xi^2}{2} \sum_{\nu} \left| \bar{\eta}_0^{(2k_1,\nu)} \right|^4 \quad (\text{F35})$$

$$+ \epsilon^2 \Xi^2 \sum_{\nu} \left| \bar{\eta}_{\frac{1}{2}(k_1-k_2)}^{(k_1+k_2,\nu)} \right|^4$$

$$+ \epsilon^4 \frac{\Xi^2}{2} \sum_{\nu} \left| \bar{\eta}_{k_2-k_1}^{(2k_2,\nu)} \right|^2 \left| \bar{\eta}_0^{(2k_2,\nu)} \right|^2,$$

$$N_{k_2} \simeq \epsilon^2 \Xi + \epsilon^4 \frac{\Xi^2}{2} \sum_{\nu} \left| \bar{\eta}_0^{(2k_2,\nu)} \right|^4 \quad (\text{F36})$$

$$+ \epsilon^2 \Xi^2 \sum_{\nu} \left| \bar{\eta}_{\frac{1}{2}(k_1-k_2)}^{(k_1+k_2,\nu)} \right|^4$$

$$+ \frac{\Xi^2}{2} \sum_{\nu} \left| \bar{\eta}_{k_2-k_1}^{(2k_1,\nu)} \right|^2 \left| \bar{\eta}_0^{(2k_1,\nu)} \right|^2.$$

For $k_1 = k_2 \equiv k_P$, we use the single-pump results (F30)–(F31), where we need to replace $|\mathcal{P}|^2 \rightarrow |\mathcal{P}|^2 (1 + \epsilon^2)$, yielding

$$N_{2k_P,\nu} \simeq (1 + \epsilon^2)^2 \frac{\Xi^2}{2} \left| \bar{\eta}_0^{(2k_P,\nu)} \right|^2, \quad (\text{F37})$$

$$N_{k_P} \simeq (1 + \epsilon^2) \Xi + (1 + \epsilon^2)^2 \frac{\Xi^2}{2} \sum_{\nu} \left| \bar{\eta}_0^{(2k_P,\nu)} \right|^4 \quad (\text{F38})$$

Appendix G: Sums over Products of $\left| \bar{\eta}_q^{(K\nu)} \right|^2$

In this paper, we encounter sums of the form

$$\sum_{\nu} \left| \bar{\eta}_q^{(K\nu)} \right|^4 = \left| \bar{\eta}_q^{(K,\text{BS})} \right|^4 + \sum_p \left| \bar{\eta}_q^{(Kp)} \right|^4 \quad (\text{G1})$$

$$\equiv \begin{cases} Q_q^{(\text{bg})} + Q_q^{(\text{dir})} & U = 0 \\ R_q^{(\text{bg})} + R_q^{(\text{dir})} + R_q^{(\text{BS})} & U \gg \gamma_0 \end{cases}.$$

Exploiting the symmetry properties, we can further write

$$\sum_p \left| \bar{\eta}_q^{(Kp)} \right|^4 = 2 \cdot \sum_{p>0} \left| \bar{\eta}_q^{(Kp)} \right|^4 + \left| \bar{\eta}_q^{(K,p=0)} \right|^4 \quad (\text{G2})$$

$$= 2 \cdot \left(\sum_{p>0, p \neq q} \left| \bar{\eta}_q^{(Kp)} \right|^4 + \left| \bar{\eta}_q^{(Kq)} \right|^4 \right) + \left| \bar{\eta}_q^{(K,p=0)} \right|^4.$$

Here, the first part (the sum over $p > 0$ but $p \neq q$) represents the contribution from the “background fluorescence” (“bg”), whereas the second term ($p = q$) stems from the emission via a “direct channel” (“dir”). The last

term refers to a $p = 0$ -relative wavefunction and therefore vanishes for both $U = 0$ and $U \gg \gamma_0$ (see also Sec. II B).

The relevant quantities to be calculated are

$$Q_q^{(\text{bg})} \equiv 2 \sum_{p>0, p \neq q} \left| \bar{\eta}_q^{(Kp)} \right|^4 \quad \text{for } U = 0, \quad (\text{G3})$$

$$R_q^{(\text{bg})} \equiv 2 \sum_{p>0, p \neq q} \left| \bar{\eta}_q^{(Kp)} \right|^4 \quad \text{for } U \gg \gamma_0, \quad (\text{G4})$$

$$R_q^{(\text{dir})} \equiv 2 \left| \bar{\eta}_q^{(Kq)} \right|^4 \quad \text{for } U \gg \gamma_0, \quad (\text{G5})$$

$$R_q^{(\text{BS})} \equiv \left| \bar{\eta}_q^{(K, \text{BS})} \right|^4 \quad \text{for } U \gg \gamma_0, \quad (\text{G6})$$

$$Q_q^{(\text{cross})} \equiv \sum_p \left| \bar{\eta}_0^{(Kp)} \right|^2 \left| \bar{\eta}_q^{(Kp)} \right|^2 \quad \text{for } U = 0 \quad (\text{G7})$$

$$= 2 \left(\sum_{p>0, p \neq q} \left| \bar{\eta}_0^{(Kp)} \right|^2 \left| \bar{\eta}_q^{(Kp)} \right|^2 + \underbrace{\left| \bar{\eta}_0^{(Kp)} \right|^2 \left| \bar{\eta}_q^{(Kq)} \right|^2}_{U=0} \right)$$

$$= 2 \sum_{p>0, p \neq q} \left| \bar{\eta}_0^{(Kp)} \right|^2 \left| \bar{\eta}_q^{(Kp)} \right|^2,$$

$$R_q^{(\text{cross})} \equiv \sum_p \left| \bar{\eta}_0^{(Kp)} \right|^2 \left| \bar{\eta}_q^{(Kp)} \right|^2 \quad \text{for } U \gg \gamma_0, \quad (\text{G8})$$

$$R_q^{(\text{cross BS})} \equiv \left| \bar{\eta}_0^{(K, \text{BS})} \right|^2 \left| \bar{\eta}_q^{(K, \text{BS})} \right|^2 \quad \text{for } U \gg \gamma_0. \quad (\text{G9})$$

Inserting the expressions for the momentum distributions from Sec. II C 2, we ultimately have to calculate ($M \gg 1$)

$$Q_q^{(\text{bg})} = \frac{32}{M^4} \sum_{p>0, p \neq q} \frac{1}{\tan^4 \left[\frac{1}{2} (p - q) a \right]} \times \left(1 - \delta_{\left[\frac{(p-q)Na}{2\pi} \right]_2, 0} \right), \quad (\text{G10})$$

$$R_q^{(\text{bg})} = \frac{32}{M^4} \sum_{p>0, p \neq q} \frac{\cos^4 \left[\frac{1}{2} (p + q) a \right]}{\sin^4 \left[\frac{1}{2} (p - q) a \right]} \times \left(1 - \delta_{\left[\frac{(p-q)Na}{2\pi} \right]_2, 0} \right), \quad (\text{G11})$$

$$R_q^{(\text{dir})} = 2 \sin^4(qa), \quad (\text{G12})$$

$$R_q^{(\text{BS})} = \frac{16}{M^2} \cos^4(qa), \quad (\text{G13})$$

$$Q_q^{(\text{cross})} = \frac{32}{M^4} \sum_{p>0, p \neq q} \frac{1}{\tan^2 \left(\frac{pa}{2} \right)} \frac{1}{\tan^2 \left[\frac{1}{2} (p - q) a \right]} \quad (\text{G14})$$

$$\times \left(1 - \delta_{\left[\frac{(p-q)Na}{2\pi} \right]_2, 0} \right), \quad (\text{G15})$$

$$R_q^{(\text{cross BS})} = \frac{16}{M^2} \cos^2(qa) \times \left(1 - \delta_{\left[\frac{(p-q)Na}{2\pi} \right]_2, 0} \right), \quad (\text{G16})$$

The remaining lattice sums can be performed for $M \gg 1$ as follows. We explain the procedure for Eq. (G10). The other quantities can be obtained in a similar manner. Defining $\delta \equiv 2\pi/aM \ll 1$ and rewriting $p = q + \delta \cdot n$ (n is an integer), we essentially need to calculate

$$Q_q^{(\text{bg})} = \frac{2\delta^4 a^4}{\pi^4} \sum_n' \frac{1}{\tan^4 \left(\frac{\delta a}{2} \cdot n \right)}, \quad (\text{G17})$$

where the sum runs over those odd values of n such that all wavenumbers from $0 \rightarrow q - \delta$ as well as from $q + \delta \rightarrow \pi/a$ are covered. Since $M \gg 1$, this expression can be expanded into a Taylor series in δ (around $\delta = 0$). In the limit $M \gg 1$, only terms of order δ^0 remain, yielding

$$Q_q^{(\text{bg})} = \frac{2a^4}{\pi^4} \cdot \frac{16}{a^4} \cdot (2 - \delta_{q0}) \cdot \underbrace{\sum_{n=0}^{\infty} \frac{1}{(2n+1)^4}}_{=\frac{\pi^4}{96}} \quad (\text{G18})$$

$$= \frac{1}{3} (2 - \delta_{q0}).$$

If $q \neq 0$, then there are (for $M \rightarrow \infty$) infinitely many wavenumbers on either side of q (i.e., from $0 \rightarrow q - \delta$ as well as from $q + \delta \rightarrow \pi/a$). Hence, we have a factor of 2 in front of the sum over all odd values. In contrast to this, if $q = 0$, there is only a single interval (and therefore we just have the factor of 1).

The other quantities can be calculated in a similar manner, yielding

$$R_q^{(\text{bg})} = \cos^4(qa) Q_q^{(\text{bg})}, \quad (\text{G19})$$

$$Q_q^{(\text{cross})} = \frac{1}{3} \delta_{q0} = Q_q^{(\text{bg})} \delta_{q0}, \quad (\text{G20})$$

$$R_q^{(\text{cross})} = Q_q^{(\text{bg})} \delta_{q0}. \quad (\text{G21})$$

Note that $R_{q=0}^{(\text{cross})} = Q_{q=0}^{(\text{cross})} = R_{q=0}^{(\text{bg})} = Q_{q=0}^{(\text{bg})} = 1/3$.

- [1] K. Winkler, G. Thalhammer, F. Lang, R. Grimm, J. Hecker Denschlag, A. J. Daley, A. Kantian, H. P. Büchler, and P. Zoller, *Nature* **441**, 853 (2006).
 [2] T. Fukuhara, P. Schnau, M. Endres, S. Hild, M. Cheneau, I. Bloch, and C. Gross, *Nature* **502**, 76 (2013).

- [3] D. Jacksch and P. Zoller, *Annals of Physics* **315**, 52 (2005).
 [4] E. Vetsch, D. Reitz, G. Sague, R. Schmidt, S. T. Dawkins, and A. Rauschenbeutel, *Phys. Rev. Lett.* **104**, 203603 (2010).

- [5] A. Kay and D. G. Angelakis, *Europhys. Lett.* **84**, 20001 (2008).
- [6] G. Zhu, S. Schmidt, and J. Koch, *New J. Phys.* **15**, 115002 (2013).
- [7] M. J. Hartmann, F. G. S. L. Brandão, and M. B. Plenio, *Laser & Photon. Rev.* **2**, 527 (2008).
- [8] A. W. Schell, J. Kaschke, J. Fischer, R. Henze, J. Wolters, M. Wegener, and O. Benson, *Sci. Rep.* **3**, 1577 (2013).
- [9] F. Herrera, Y. Cao, S. Kais, K. B. Whaley, *New J. Phys.* **16**, 075001 (2014).
- [10] M. Valiente and D. Petrosyan, *J. Phys. B: At. Mol. Opt. Phys.* **41**, 161002 (2008).
- [11] M. Valiente and D. Petrosyan, *J. Phys. B: At. Mol. Opt. Phys.* **42**, 121001 (2009).
- [12] V. M. Agranovich, M. D. Galanin, and O. Glebov, *Electronic excitation energy transfer in condensed matter*, North-Holland Amsterdam (1982).
- [13] F. C. Spano, V. Agranovich, and S. Mukamel, *J. Chem. Phys.* **95**, 1400 (1991).
- [14] F. C. Spano, *Chem. Phys. Lett.* **234**, 29 (1995).
- [15] M. Ganahl, E. Rabel, F. H. L. Essler, and H. G. Evertz, *Phys. Rev. Lett.* **108**, 077206 (2012).
- [16] P. Longo, A. D. Greentree, K. Busch, and J. H. Cole, *Phys. Lett. A* **377**, 1242 (2013).
- [17] P. Longo and J. Evers, *Phys. Rev. Lett.* **112**, 193601 (2014).
- [18] H. Bethe, *Z. Phys.* **71**, 205 (1932).
- [19] C. Weitenberg, P. Schauß, T. Fukuhara, M. Cheneau, M. Endres, I. Bloch, and Stefan Kuhr, *Phys. Rev. Lett.* **106**, 215301 (2011).
- [20] D. Porras and J. I. Cirac, *Phys. Rev. A* **78**, 053816 (2008).
- [21] B. Olmos and I. Lesanovsky, *Phys. Rev. A* **82**, 063404 (2010).
- [22] I. B. Mekhov and H. Ritsch, *J. Phys. B: At. Mol. Opt. Phys.* **45**, 102001 (2012).
- [23] L. Jin, M. Macovei, and J. Evers, arXiv:1202.0699
- [24] B. W. Adams, C. Buth, S. M. Cavaletto, J. Evers, Z. Harman, C. H. Keitel, A. Palffy, A. Picon, R. Röhlsberger, Y. Rostovtsev, and K. Tamasaaku, *J. Mod. Opt.* **60**, 2 (2013).
- [25] R. Röhlsberger, *Nuclear Condensed Matter Physics with Synchrotron Radiation*, Springer Tracts in Modern Physics, Vol. **208** (Springer Berlin Heidelberg, 2005).
- [26] O. Kocharovskaya, R. Kolesov, and Y. Rostovtsev, *Phys. Rev. Lett.* **82**, 3593 (1999).
- [27] A. Palffy, C. H. Keitel, and J. Evers, *Phys. Rev. Lett.* **103**, 017401 (2009).
- [28] T. J. Bürvenich, J. Evers, and C. H. Keitel, *Phys. Rev. Lett.* **96**, 142501 (2006).
- [29] T. J. Bürvenich, J. Evers, and C. H. Keitel, *Phys. Rev. C* **74**, 044601 (2006).
- [30] N. ten Brinke, R. Schützhold, and D. Habs, *Phys. Rev. A* **87**, 053814 (2013).
- [31] W.-T. Liao, A. Palffy, and C. H. Keitel, *Phys. Rev. Lett.* **109**, 197403 (2012).
- [32] K. P. Heeg and J. Evers, *Phys. Rev. A* **88**, 043828 (2013).
- [33] Y. V. Shvydko, T. Hertrich, U. van Bürck, E. Gerdau, O. Leupold, J. Metge, H. D. Rüter, S. Schwendy, G. V. Smirnov, W. Potzel, and P. Schindelmann, *Phys. Rev. Lett.* **77**, 3232 (1996).
- [34] R. Coussement, Y. Rostovtsev, J. Odeurs, G. Neyens, H. Muramatsu, S. Gheysen, R. Callens, K. Vyvey, G. Kozyreff, P. Mandel, R. Shakhmuratov, and O. Kocharovskaya, *Phys. Rev. Lett.* **89**, 107601 (2002).
- [35] R. N. Shakhmuratov, F. Vagizov, J. Odeurs, and O. Kocharovskaya, *Phys. Rev. A* **80**, 063805 (2009).
- [36] R. Röhlsberger, K. Schlage, B. Sahoo, S. Couet, and R. Ruffer, *Science* **328**, 1248 (2010).
- [37] R. N. Shakhmuratov, F. Vagizov, and O. Kocharovskaya, *Phys. Rev. A* **84**, 043820 (2011).
- [38] R. Röhlsberger, H.-C. Wille, K. Schlage, and B. Sahoo, *Nature* **482**, 199 (2012).
- [39] K. P. Heeg, H.-C. Wille, K. Schlage, T. Guryeva, D. Schumacher, I. Uschmann, K. S. Schulze, B. Marx, T. Kämpfer, G. G. Paulus, R. Röhlsberger, and J. Evers, *Phys. Rev. Lett.* **111**, 073601 (2013).
- [40] F. Vagizov, V. Antonov, Y. V. Radeonychev, R. N. Shakhmuratov, and O. Kocharovskaya, *Nature* **508**, 80 (2014).
- [41] Q.-F. Zhan, J.-H. Gao, Y.-Q. Liang, N.-L. Di, and Z.-H. Cheng, *Phys. Rev. B* **72**, 024428 (2005).
- [42] K. P. Heeg, J. Haber, D. Schumacher, L. Bocklage, H.-C. Wille, K. S. Schulze, R. Loetzsch, I. Uschmann, G. G. Paulus, R. Ruffer, R. Röhlsberger, and J. Evers, arXiv:1409.0365 [quant-ph].
- [43] R. Mössbauer, *Z. Phys.* **151**, 124 (1958).
- [44] M. Kalvius and P. Kienle (Eds.), *The Rudolf Mössbauer Story*, Springer, Heidelberg (2012).
- [45] Y. Li, J. Evers, H. Zheng, and S.-Y. Zhu, *Phys. Rev. A* **85**, 053830 (2012).
- [46] R. H. Dicke, *Phys. Rev.* **93**, 99 (1954).
- [47] M. Gross and S. Haroche, *Phys. Rep.* **93**, 301 (1982).
- [48] C. S. Hofmann, G. Günter, H. Schempp, M. Robert-de-Saint-Vincent, M. Gärtner, J. Evers, S. Whitlock, and M. Weidemüller, *Phys. Rev. Lett.* **110**, 203601 (2013).
- [49] D. C. Brody, *J. Phys. A: Math. Theor.* **47**, 035305 (2014).
- [50] This procedure is equivalent to setting up a Lindblad equation with respect to the bare atomic basis in the first place and then diagonalizing the coherent part.
- [51] Note that by redefining the phase shift as $\delta'_{Kp} = -\delta_{Kp}/2 + \pi/2$ our ansatz (17) for the relative wavefunction can be brought into the form $\Psi_x^{(Kp)} \propto \sin(pa|x| + \delta'_{Kp})$, which is often used in the context of cold-atom scattering.
- [52] R. J. Glauber, *Phys. Rev.* **130**, 2529 (1963).
- [53] L. Mandel and E. Wolf, *Optical Coherence and Quantum Optics*, Cambridge University Press (1995).
- [54] Z. Ficek and S. Swain, *Quantum Interference and Coherence*, Springer (2005).
- [55] M. Orszag, *Quantum Optics*, Springer (2000).
- [56] D. Meschede, *Optics, Light and Lasers: The Practical Approach to Modern Aspects of Photonics and Laser Physics*, Wiley-VCH (2007).
- [57] M. Wiegand, *Optics Communications* **36**, 297 (1981).
- [58] Z. Ficek, R. Tanas, and S. Kielich, *Phys. Rev. A* **29**, 2004 (1984).
- [59] In the expressions for $g^{(2)}(0)$ in Refs. [57, 58], we neglect the “cooperativity parameters” and assume $(1+a)^2 + b^2 \approx 1$ (assuming the inter-atomic dipole-dipole coupling to be small). Furthermore, the angle-dependence which is encoded in the cos-terms drops out for the special geometry considered in Sec. IV C.
- [60] J. G. Cordes and J. A. Chevary, *J. Phys. B: At. Mol. Phys.* **17**, 1913 (1984).
- [61] F. Miftasani and P. Machnikowski, arXiv:1407.4603